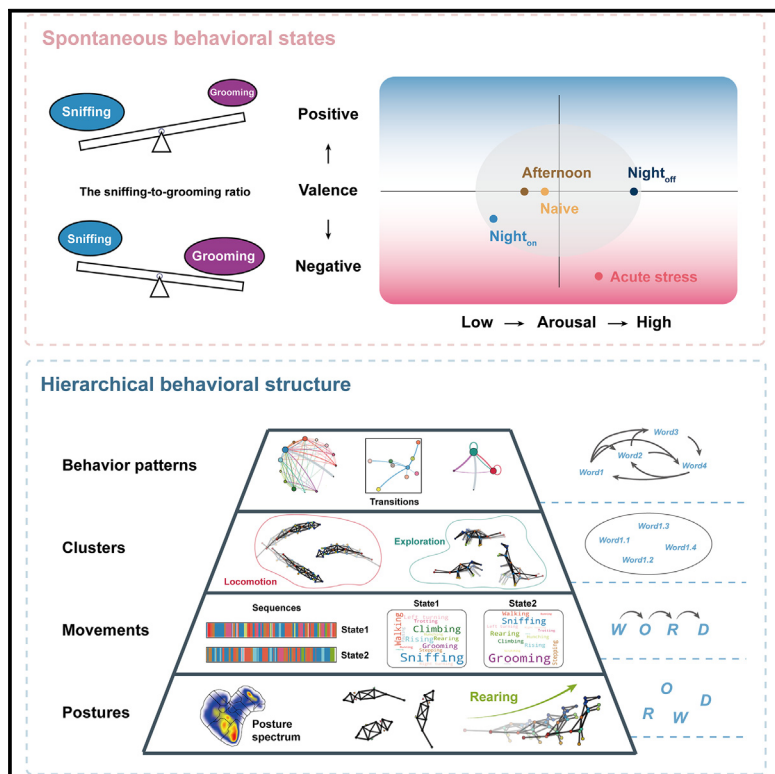


Hierarchical behavioral analysis framework as a platform for standardized quantitative identification of behaviors

Graphical abstract



Highlights

- Sniffing serves as the hub node for the movement transition of spontaneous behavior patterns
- The sniffing-to-grooming ratio evaluates behavioral states in a high-throughput manner
- Emotional states, circadian rhythms, and lighting conditions influence spontaneous behavior
- A data-driven approach for segmenting regions captures the spatial preferences of mice

Authors

Jialin Ye (叶家霖), Yang Xu (徐阳),
Kang Huang (黄康), Xinyu Wang (王新雨),
Liping Wang (王立平), Feng Wang (王枫)

Correspondence

lp.wang@siat.ac.cn (L.W.),
feng.wang@siat.ac.cn (F.W.)

In brief

Ye et al. develop a hierarchical behavioral analysis framework that reveals the high-dimensional features and organizational logic of spontaneous behaviors in male and female mice. They identify sniffing as a hub node in this structure, and the sniffing-to-grooming ratio effectively distinguishes between different spontaneous behavioral states in a high-throughput manner.



Article

Hierarchical behavioral analysis framework as a platform for standardized quantitative identification of behaviors

Jialin Ye (叶家霖),^{1,2,3} Yang Xu (徐阳),^{1,2,3} Kang Huang (黄康),^{1,2,3} Xinyu Wang (王新雨),^{1,2,3} Liping Wang (王立平),^{1,2,3,4,*} and Feng Wang (王枫)^{1,2,3,4,5,*}

¹Shenzhen Key Laboratory of Neuropsychiatric Modulation, Shenzhen-Hong Kong Institute of Brain Science, Shenzhen Institutes of Advanced Technology, Chinese Academy of Sciences, Shenzhen 518055, China

²CAS Key Laboratory of Brain Connectome and Manipulation, the Brain Cognition and Brain Disease Institute, Shenzhen Institutes of Advanced Technology, Chinese Academy of Sciences, Shenzhen 518055, China

³Guangdong Provincial Key Laboratory of Brain Connectome and Behavior, the Brain Cognition and Brain Disease Institute, Shenzhen Institutes of Advanced Technology, Chinese Academy of Sciences, Shenzhen 518055, China

⁴University of Chinese Academy of Sciences, Beijing 101408, China

⁵Lead contact

*Correspondence: lp.wang@siat.ac.cn (L.W.), feng.wang@siat.ac.cn (F.W.)

<https://doi.org/10.1016/j.celrep.2025.115239>

SUMMARY

Behavior is composed of modules that operate based on inherent logic. Understanding behavior and its neural mechanisms is facilitated by clear structural behavioral analysis. Here, we developed a hierarchical behavioral analysis framework (HBAF) that efficiently reveals the organizational logic of these modules by analyzing high-dimensional behavioral data. By creating a spontaneous behavior atlas for male and female mice, we discovered that spontaneous behavior patterns are hardwired, with sniffing serving as the hub node for movement transitions. The sniffing-to-grooming ratio accurately distinguished the spontaneous behavioral states in a high-throughput manner. These states are influenced by emotional status, circadian rhythms, and lighting conditions, leading to unique behavioral characteristics, spatiotemporal features, and dynamic patterns. By implementing the straightforward and achievable spontaneous behavior paradigm, HBAF enables swift and accurate assessment of animal behavioral states and bridges the gap between a theoretical understanding of the behavioral structure and practical analysis using comprehensive multidimensional behavioral information.

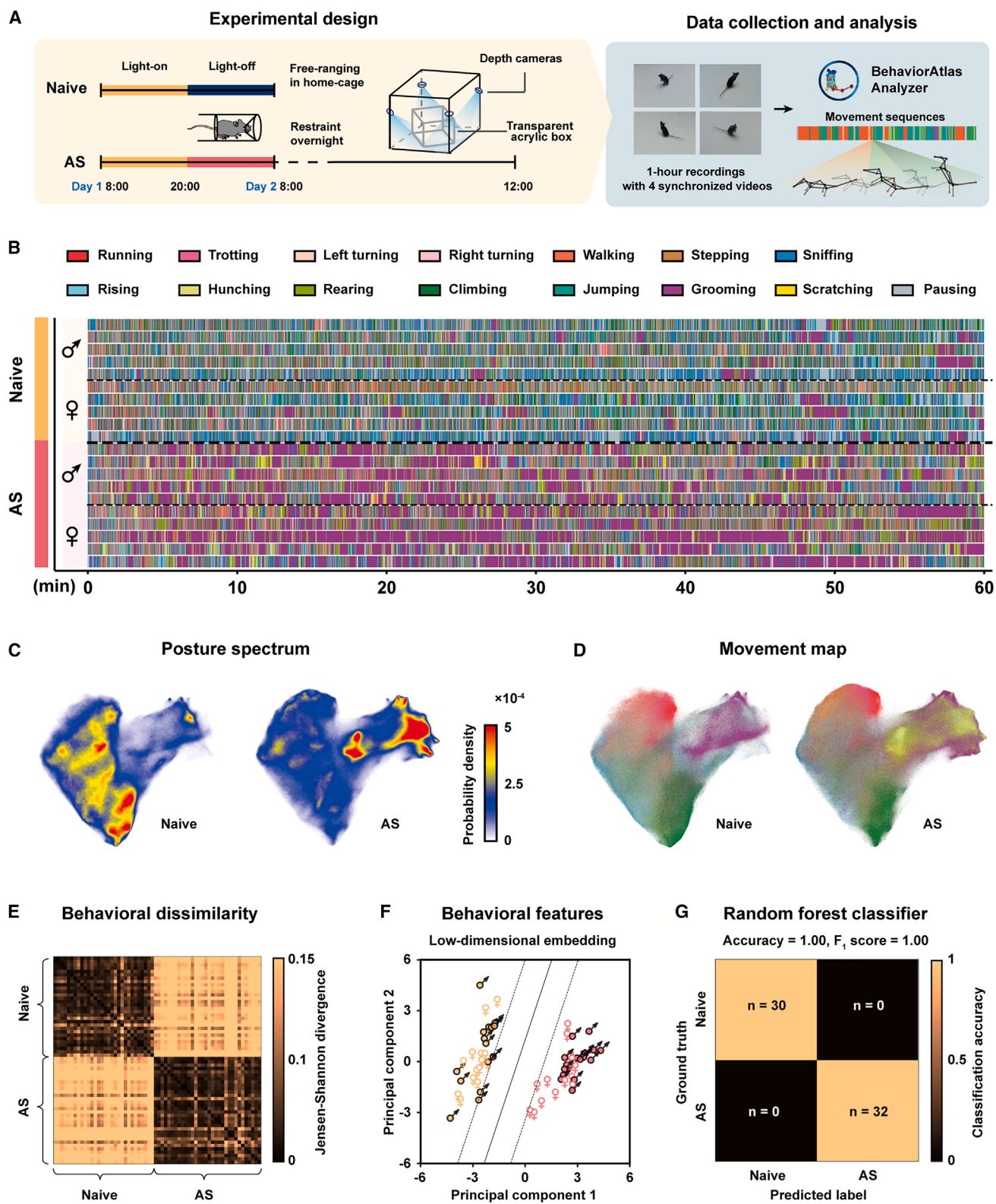
INTRODUCTION

Quantifying behavior is challenging^{1–4} due to the lack of a universal computational ethology conceptual framework capable of analyzing and quantifying multi-scale, complex behavioral dynamics.^{5–7} Behavior consists of movement components that combine probabilistically^{8–10} according to specific rules,^{11–13} with transitions between behavioral states^{14,15} driven by the nervous system. Spatial and temporal patterns of behavioral modules are crucial for generating appropriate behavior^{12,16} and reflect rule-guided behaviors between organisms and their environments.^{17,18} The theory of ethome structure has been introduced to comprehensively describe the hierarchical structure of natural behaviors.^{2,5} This involves extracting time-series data of postures and converting them into dynamic representations to identify specific behaviors. Advances in machine learning for pose estimation^{19–26} and behavior segmentation^{27–29} have enabled the decomposition of continuous behavior into quantifiable modules.^{6,13,17,30,31} Unified foundation models³² and open-source platforms⁷ now offer infrastructure

for applying these techniques, particularly in dissecting behavior affected by stress. However, the absence of a corresponding hierarchical framework for behavior analysis limits the practical application of this theoretical knowledge.

Spontaneous behavior, defined as actions occurring without conscious intent or external stimuli, is crucial for health maintenance and body regulation.^{33,34} It reflects the animal's internal state,^{35–38} with changes indicating potential health issues such as pain³⁹ and toxin exposure⁴⁰; conditions like inter-ictal periods of seizures,⁴¹ stroke recovery,⁴² and autism⁴³; as well as acute stress (AS).^{44,45} In mice, spontaneous behavior includes locomotion,^{46,47} self-grooming,^{48–50} and exploration.^{51–53} Self-grooming, a natural behavior across species,⁵⁴ is vital in rodents and often increases in both high- and low-stress situations.^{55,56} Sniffing, an innate exploratory behavior^{57,58} helps rodents understand their surroundings^{59–61} and aids resource finding,^{62,63} social communication,^{64,65} and threat evaluation.^{66–69} By considering behavior as a continuous process,² changes can be detected through dynamic nervous system patterns.^{5,70} Nevertheless, the understanding of spontaneous behavior components and





(legend on next page)

organizational principles, including grooming and sniffing, remains limited.

To establish an accessible and explainable framework for analyzing behaviors, we developed a hierarchical behavioral analysis framework (HBAF). Using a simple spontaneous behavior paradigm, HBAF enables standardized, rapid, and hierarchical quantitative analysis, improving the accuracy and efficiency of behavioral identification. Our study systematically examined spontaneous behavior in male and female mice, including posture and its kinematics, movements and clusters, spatiotemporal characteristics, and organizational logic in an open-field arena. The findings revealed that sniffing serves as a hub node for movement transitions under different conditions, with behavioral characteristics and transition frequencies influenced by emotional status, circadian rhythms, and light conditions. These factors shape distinct behavioral patterns. The sniffing-to-grooming ratio accurately differentiated behavioral states in a high-throughput manner. HBAF provides a comprehensive platform for understanding animal behaviors, bridging the gap between the theoretical knowledge of the behavioral structure and practical analysis.

RESULTS

Analyzing dimensional reduction based on high-dimensional postures distinguishes spontaneous behavioral phenotypes

To identify spontaneous behavioral phenotypes, multiview video streams were decomposed into sub-second clips based on dynamic postural features and then unsupervised clustered into 40 movement modules³¹ (Figures 1A and S1). After supervised labeling and merging, 15 different movements were identified (Figures 1B and S2F; Table S1) and categorized into 4 biologically relevant clusters (Figure S2F; Table S1). The reliability and accuracy of the movement recognition and classification were evidenced by the clustering performance of modules obtained through unsupervised clustering (Figures S2A and S2B) and the consistency of postures and kinematic features of identified movements (Figures S2C–S2E). Significant differences were observed in the movement sequences (Figure 1B), posture probabilistic density map (Figure 1C), and posture-specific movement expression (Figure 1D) between the naive and AS (Acute

stress, mice were restrained in a tube overnight) groups as well as nocturnal behaviors under light-on (Night_{on}) and light-off ($\text{Night}_{\text{off}}$) conditions (Figure S3A). The movement fraction pattern indicated high within-group similarity and clear between-group differences (Figure 1E), accurately clustering group-specific behavioral features in low-dimensional space (Figure 1F) and predicting group labels (Figure 1G). Unlike single parameters, movement repertoires reduced from high-dimensional posture data effectively distinguished spontaneous behavioral phenotypes (Figure S3B), highlighting their utility in behavioral analysis.

Dynamic postural kinematics form the foundation of behavioral structure

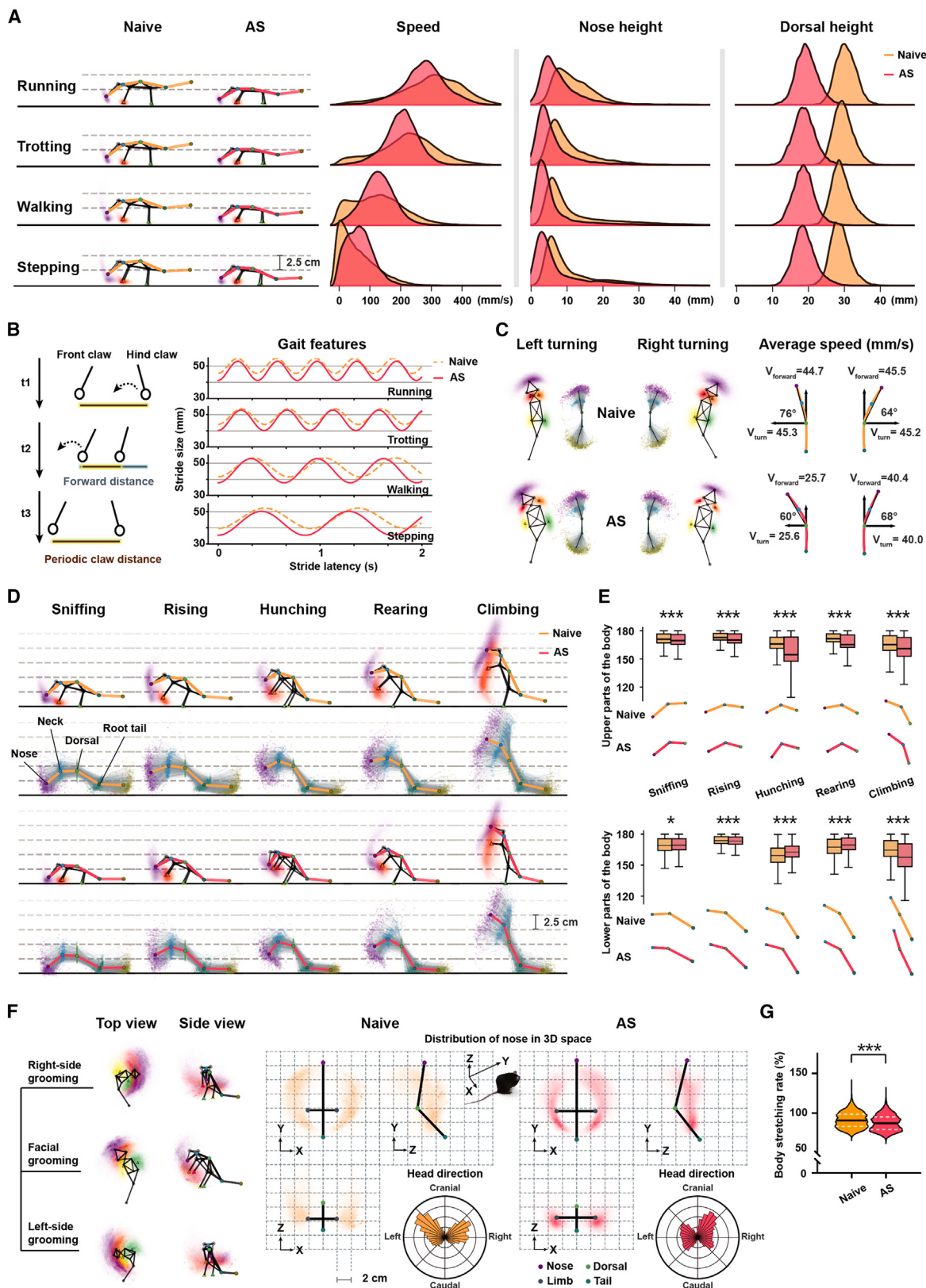
Behavior consists of movements made up of coordinated postures involving rapid body changes in 3D space.⁴ Subtle postural changes, such as kyphosis,⁷¹ sighing,^{72,73} and repetitive hand movements,⁷⁴ are observed in humans during anxiety states but are challenging to distinguish. To address this, we developed an algorithm to extract detailed postural kinematics from BehaviorAtlas data. In mice exposed to AS, locomotion showed reduced dorsal height (Figure 2A; Table S2), shorter and faster strides (Figure 2B), and decreased turning speed and amplitude (Figure 2C). During exploration, AS mice exhibited body contraction with lower average height (Figure 2D) and increased spine bending (Figure 2E). Additionally, the algorithm successfully identifies unique skeletal kinematic features during grooming, scratching, and pausing (Figure S2F; Table S2). For instance, in AS mice, there was not only a greater range of head movement toward the hindquarters (Figure 2F) but also a higher level of body contraction (Figure 2G). These results suggest that AS mice mimic stress-related postural changes in humans. The identified parameters could aid in detecting progressive movement disorders like Parkinson's disease and compulsive postures, offering a foundation for early diagnostic methods.

Movements and clusters can identify diversity in behavioral states

Movements are the fundamental units of animal behavior, grouped (e.g., walking and running as locomotion) and influenced by internal or external events.² AS affects mouse behavior, such as defensive behavior,^{75–77} food intake,^{78–80} sleep regulation,^{81,82} and spontaneous behavior,^{83,84} reducing locomotion

Figure 1. AS influences spontaneous behavioral characteristics

- (A) Experimental design and data processing (see also Figure S1). The spontaneous behaviors of all animals were captured in the open field for 1 h. Naive group: untreated mice, observations were conducted between 8:00 and 12:00 (light on). Acute stress (AS) group: mice were restrained from 20:00 until 8:30 the next day, and observations were conducted between 8:30 and 9:30 (light on). Zeitgeber time (ZT): ZT0 = 8:00, ZT12 = 20:00.
- (B) Ethograms of 15 movements in 60 min for 5 representative mice for each sex (see also Figure S2F and Table S1).
- (C) The MotionMapper algorithm³⁰ was used to generate a probability density map of the posture spectrum. In this map, each frame's normalized skeletons were compared in a common feature space. Poses that were closer together on the map indicate a higher similarity, and areas of higher density represent poses that occurred more frequently (see also Figure S3).
- (D) The movement map was generated by mapping the posture spectrum with movement labels assigned by BehaviorAtlas³¹ in each frame (see also Figure S3).
- (E) The dissimilarities in movement fraction distribution between pairwise mice, with the Jensen-Shannon divergence (JSD) values utilized to quantify the similarity. The higher values (lighter color in the heatmap) indicate greater dissimilarity of behavioral repertoires (see also Figure S4).
- (F) Embedding 15-dimensional movement fractions into a low-dimensional space using principal-component analysis (PCA) to represent the behavioral features. The solid line is the decision boundary identified by a support vector machine linear model (see also Figure S4).
- (G) Confusion matrix depicting the accuracy of a random forest classifier trained on 15-dimensional movement fractions to predict group labels. The model's performance was evaluated by stratified 10-fold cross-validation. For the naive group, $n = 15$ for each sex; for the AS group, $n = 16$ for each sex (see also Figure S4).



(legend on next page)

distance⁸⁵ and central-area activity^{82,86} in the open field test. Our study found significant differences in 12 movement fractions in both male and female mice between the naive and AS groups (Figure 3A). AS mice exhibited decreased locomotion and exploration (Figure 3B) but increased grooming (Figure 3A) compared to naive mice, along with a distinctive display of scratching, which was almost absent in naive mice. Moreover, AS mice showed a decrease in both the proportion and frequency of sniffing, while grooming increased significantly (Figures 3A and 3C). The sniffing-to-grooming ratio of AS mice compared to the other group of mice showed significant differences (Figure 3D), along with very high predictive accuracy (Figure 3E), making the sniffing-to-grooming ratio a reliable indicator of abnormal behavioral states with high predictive accuracy.

Rodent behavior also varies by time of day, influenced by the sleep cycle,^{87,88} feeding and drinking regularity,⁸⁹ and reproduction behavior.^{90,91} Our findings revealed that mice exhibit highly similar behavioral characteristics in the morning and afternoon, except for female mice displaying less stepping and more rearing in the afternoon (Figures S4A–S4E). Significant differences in movement fractions were noted between morning and night with the lights off (Figures S4F–S4J). Changing in lighting at night had a greater impact than circadian rhythms (Figures S4K–S4O), with rising and left turning increased under light-on circumstances, while running, trotting, walking, stepping, and hunching decreased under the light-off condition. No significant differences were found between male and female mice, except for higher trotting in the female Night_{off} group (Figure S5), or among females across estrous cycles (Figure S6). Our findings shed light on the importance of timing, lighting, and including both sexes in spontaneous behavior experiments.

Changes in behavioral states are reflected in their temporal features

The temporal pattern of spontaneous behavior in mice changed after AS.^{84,92,93} A minute-by-minute analysis of the dynamics of each movement revealed significant changes in the patterns of eight movements (Figure 4A). Compared to naive mice, AS mice exhibited a distinct time-dependent pattern of movements during left and right turning, especially in exploratory behaviors like hunching, climbing, and jumping, as well as in maintenance (Figure 4A). AS mice exhibited reduced locomotion distance per minute, with male mice showing a more pronounced decrease in total distance (Figure 4B). Analysis in 5-min blocks demon-

strated that Naive mice displayed similar population behavioral repertoires for the first 15 min, declining and diverging around 45 min (Figure 4C), while AS mice maintained high similarity from 6 to 25 min (Figure 4C). Naive mice explored in the first 15 min and rested after 45 min, whereas mice prioritize maintenance over exploration, suppressing rest (Figure 4D).

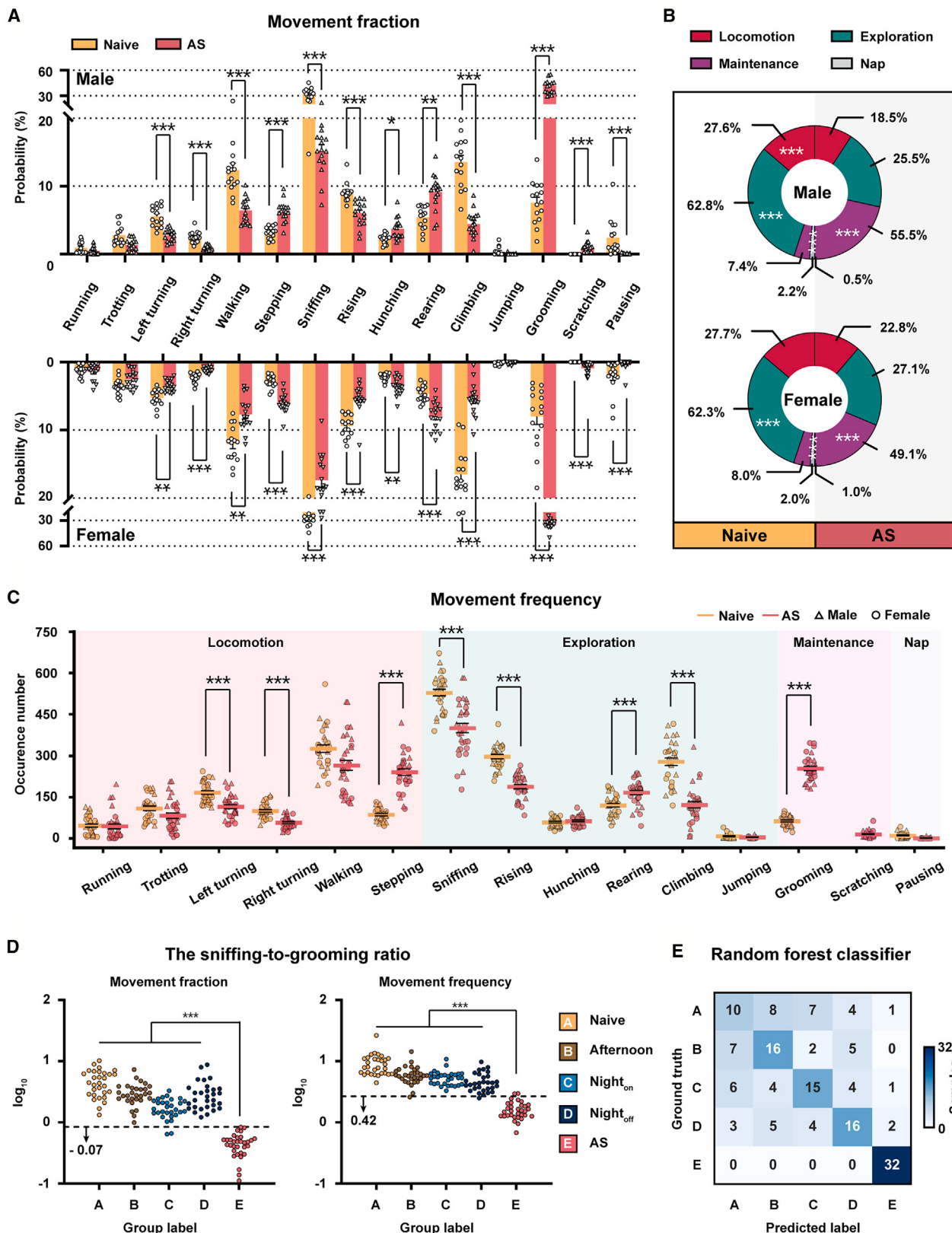
Comparing different experimental conditions showed temporal differences in movements (Figures S7A, S7D, and S7G). At nighttime, mice traveled shorter distances with lights on, especially females, and no differences in locomotion distances were observed between groups or sexes (Figures S7B, S7E, and S7H). In the first 15 min, mice focused on exploration during the morning, afternoon, and night with lights on (Figures S7C, S7F, and S7I), and during nocturnal experiments without light (Figures S7C and S7H), there was no decrease in activity similarity seen at the 45-min mark (Figure S7F). Instead, mice exhibited minimal napping throughout 60-min nocturnal activities without light, suggesting that their peak activity was during this interval. These results underscore the need for adequate acclimatization before behavioral testing, as inadequate time may affect attention, especially in longer daytime experiments.

A data-driven approach for segmenting regions effectively captures the spatial preferences of mice

AS elicits anxiety-like behaviors,^{94–96} often evaluated via the open field test.^{97,98} The traditional approach involves defining the central and perimeter areas and calculating the time spent in the central area during 10 minutes of spontaneous activity,^{97–99} but debates persist over defining the central area.^{100,101} Our data showed a significant change in spatial preference in AS mice (Figure 5A), initially staying farther from the center, which was consistent with previous findings,^{97,102} but moving closer after 50 min (Figure 5B). Using a data-driven approach, we identify natural occupancy-based central and peripheral areas (Figure S8B). Through an evaluation of the density variance within an expanding frame (Figure 5C), we calculated the central region as 35 cm, larger than the traditional 25 cm (Figure 5D). This method showed more consistent dorsal point distributions (Figures 5C, 5D, and S8C). Further analysis revealed that naive mice were more active in the central area in the initial 10 min (Figure 5E), primarily engaging in locomotion and exploration (Figure 5F). In contrast, in AS mice, the most predominant activity in these areas was locomotion and maintenance, maintenance and exploration, and maintenance and exploration,

Figure 2. Dynamic postural kinematics of movements

- (A) The average skeletons of four kinds of locomotion movements in side view (left) and the distribution of locomotion speed, nose height, and dorsal height of these movements (right). The colored scatter density heatmap illustrates the activity range of the corresponding body part.
 - (B) Gait analysis of 4 kinds of locomotion movements, including stride frequency and stride length.
 - (C) The average skeletons of turning movements in top view along with the average turning amplitude and velocity component of these two movements.
 - (D) Side view of the average skeleton and the average torso of exploration (except jumping). The average torso is represented by a line connecting the nose, neck, dorsal, root tail, and mid-tail.
 - (E) The degree of curling of the upper (from nose to neck to dorsal) and lower parts of the body (from neck to dorsal to root tail). Data are shown in the boxplot. A Mann-Whitney test was performed to evaluate the differences in the curling degree of individually selected movements between the two groups.
 - (F) Top and side views of the representative skeleton of grooming. The scatter density map compares the nose's position in 3D, and the wind rose plot shows the distribution of head orientation during grooming.
 - (G) Comparison of body stretching rate on grooming between the naive and the AS mice. 10,000 frames belonging to grooming were randomly extracted from each group. Data are visualized using a violin plot. A Mann-Whitney test was performed to evaluate the differences in body stretching rate.
- See also Figure S2F and Table S1.



(legend on next page)

respectively, during the first 10 min (Figure 5F), with a further increase in maintenance in the central area during the subsequent 50 min. The sniffing-to-grooming ratio differed significantly in AS mice, particularly in the corners, where it accurately distinguished AS from normal states (Figure 5G). This suggests that a higher sniffing-to-grooming ratio in corners during the first 10 min is significant enough to serve as a promising indicator for high-throughput identification of abnormal behavioral states. These findings call for reassessing previous conclusions about anxiety reduction based solely on time spent in the center.

Sniffing serves as the hub node for movement transition in spontaneous behavior patterns

A behavior sequence is defined as a series of ordered movements, while the inherent organizational structure of these sequences is referred to as a behavior pattern. By analyzing the transition probabilities between movements and clusters, we aimed to interpret the spontaneous behavior patterns of mice (Figure 6A). Morning and nighttime behaviors revealed variations in movement transition networks (Figure S9A), though cluster transition networks remained relatively stable (Figure S9B), reflecting a fundamental hardwired logic with movement-level diversity under different time and lighting conditions. After AS, significant changes were observed in both movement (Figure 6B) and cluster transition networks (Figure 6C), with locomotion, exploration, and maintenance increasingly transitioning to maintenance and less to exploration (Figure 6D). Furthermore, first-order entropy analysis revealed greater unpredictability in AS mice (Figure 6E), indicating unstable behavioral patterns. Nodal movement analysis revealed distinct types and connection patterns for four nodes under the mentioned conditions (Figures 6F and 6G).

We also observed changes in the connection properties of the sniffing across various experimental conditions (Figure S9D). Although the connection features varied, sniffing emerged as the most important movement in linking different movements together to form spontaneous behavior patterns (Figures 6G, S9C, and S9D), crucial for identifying environmental cues like food, predators, and mates and other ecological cues essential for survival. Despite disruptions from illumination variation (Figure S9D) or AS (Figure 6G), the stability of spontaneous behavior patterns allows for sustained environmental attention. The HBAF effectively detects abnormal behaviors by identifying abnormal

behavior patterns and the hub node movement, providing a foundation for early neuropsychiatric disorder diagnostics.

Movement transition frequencies determine the spontaneous behavior pattern

To investigate how movement transitions shape behavior patterns, we analyzed the movement transition network to predict movement sequences in spontaneous behavior. Transition and duration probabilities were calculated at 5-min intervals (Figure 7A), allowing us to simulate movement sequences based on these probabilities (Figure 7B). The simulated data closely matched the real behavior (Figure 7C), with no significant differences (Figure S10A), supported by Jensen-Shannon divergence (JSD) values and random forest predictions (Figure S10B and S10C). Swapping dynamic movement duration probabilities between naive and AS mice showed that behavior patterns are primarily encoded by movement transition probabilities (Figure 7C), with distinct transition frequencies across groups (Figure 7D).

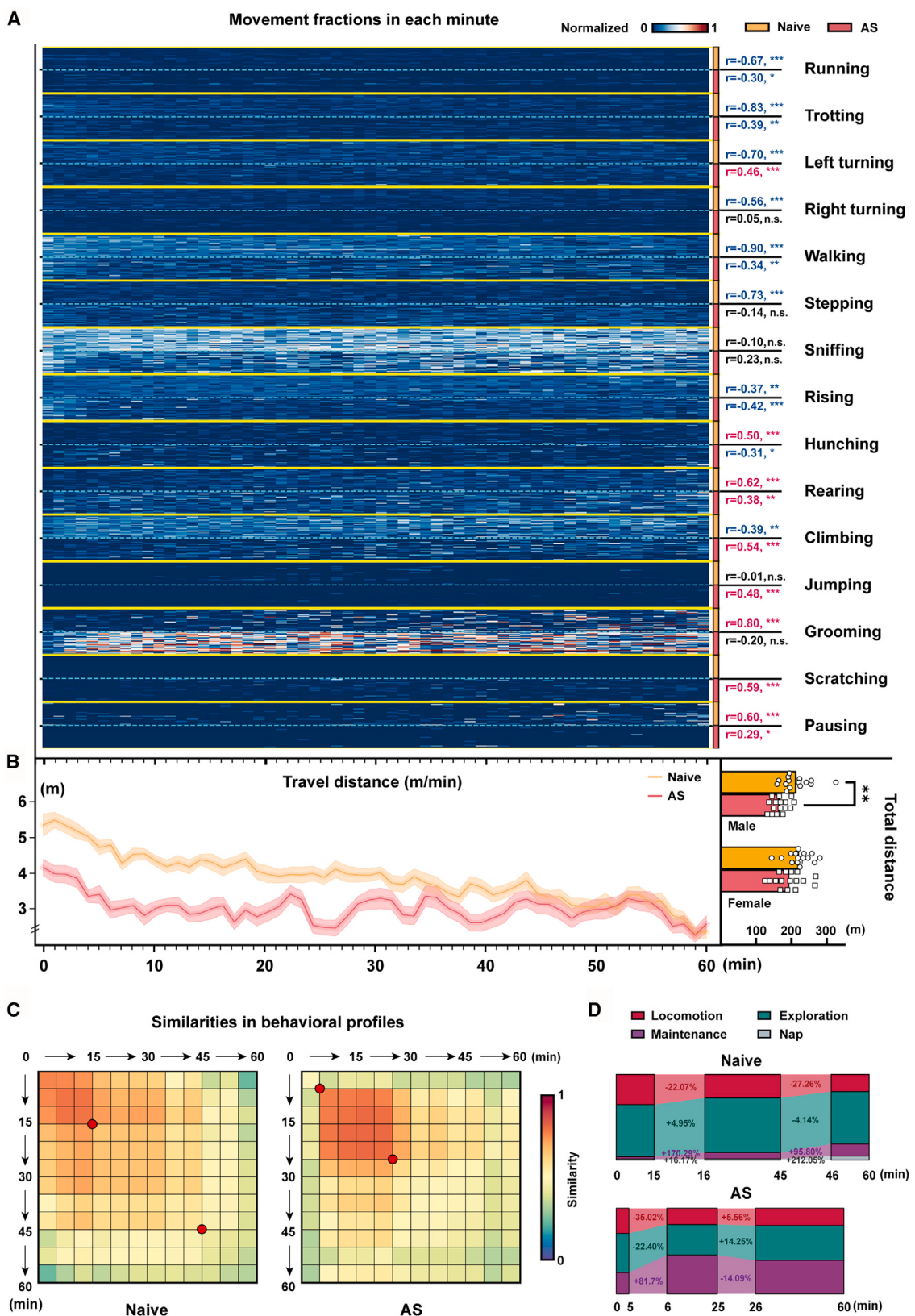
Initially, mice in an unfamiliar open field exhibited exploration-driven behavior, which decreased as they habituated and rested over time (Figure S10D). The weights of these three factors (exploration, habituation, and rest) varied across time and light conditions, explaining differences in movement transition slopes. In contrast, AS disrupted normal patterns, increasing self-attention but preserving exploratory drives, causing wave-like fluctuation in transition frequency (Figure 7D). This suggests that the movement transition network is driven by multiple innate forces, while it is also influenced by internal and external changes. A predictive model based on this dynamic network could evaluate new disease models and drug efficacy with precision and efficiency.

DISCUSSION

In this study, we developed a hierarchical behavioral analysis framework to systematically investigate behavior, moving step-by-step from posture to movement to cluster and the identification of behavioral patterns. By utilizing this framework, we revealed that the spontaneous behavioral patterns of male and female mice are hardwired, with sniffing serving as the hub node in their movement transitions of behavior patterns under different conditions. Our results showed that the spontaneous behaviors of mice vary in their characteristics and movement transition frequencies, depending on their emotional status,

Figure 3. Distinct movement features of mice in the naive and the AS groups

- (A) Comparison of movement fractions of spontaneous behavior between the naive and the AS groups. Yellow: the naive group, $n = 15$ for each sex. Red: the AS group, $n = 16$ for each sex. Normality was tested by a Shapiro-Wilk test (statistic = 0.758, $p < 0.001$) was not normally distributed. A Mann-Whitney test was performed with Bonferroni-Dunn multiple comparisons. * $p < 0.05$, ** $p < 0.01$, *** $p < 0.001$.
 - (B) Comparison of cluster proportion between the naive and the AS groups. A Mann-Whitney test was performed with Bonferroni-Dunn multiple comparisons. * $p < 0.05$, ** $p < 0.01$, *** $p < 0.001$.
 - (C) Comparison of movement frequency of spontaneous behavior between the naive and the AS groups. A Mann-Whitney test was performed with Bonferroni-Dunn multiple comparisons.
 - (D) The sniffing-to-grooming ratios are represented in terms of movement fraction (left) and frequency (right). The values are shown in the logarithm. Yellow: the naive group. Brown: the afternoon group; observations were conducted between 14:00 and 18:00 (light on). Deep blue: the Night_{off} group; observations were conducted between 20:00 and 24:00 (light off). Light blue: the Night_{on} group; observations were conducted between 20:00 and 24:00 (light on). Red: the AS group.
 - (E) Group labels were predicted by a random forest classifier trained on the ratio of sniffing to grooming, using both movement fractions and movement frequencies. Numbers in the heatmap indicated the number of mice. The model's performance was evaluated by stratified 10-fold cross-validation. For the naive, the afternoon, the Night_{on}, and the Night_{off} groups, $n = 15$ for each sex; for the AS group, $n = 16$ for each group.
- The data are presented as mean \pm SEM. The source data and statistical information are provided in Table S3.



(legend on next page)

circadian rhythms, and light conditions. These differences, driven by diverse internal and external factors, ultimately contribute to the formation of distinct behavioral patterns. The spatial preferences of AS mice exhibited significant dimorphic features over time, while the sniffing-to-grooming ratio may serve as an indicator of spontaneous behavioral states. HBAF is an accessible and explainable framework for behavioral analysis that enables not only swift and accurate assessment of animal behavioral states but also bridges the gap between a theoretical understanding of the behavioral structure and practical analysis using comprehensive multidimensional behavioral information.

HBAF was developed to analyze animal behaviors in a high-throughput manner

The behaviors exhibited by individuals are influenced by their current environmental context and a variety of internal states.¹⁵ Since 1951, when Tinbergen⁸ emphasized the significance of considering behavior from a broad perspective and viewing each issue as part of a whole, numerous researchers have extensively explored this topic and proposed several behavioral structure theories, such as behavior sequence,¹⁰³ lexical model,¹⁰⁴ fingerprint,¹⁰⁵ ethome^{2,5} etc. The concept of ethome has been introduced,¹⁰⁶ along with the idea of categorizing behavior into ethograms/activities, actions, and movements.^{2,13} In this study, we implemented the concept of behavioral structure described earlier.¹⁰⁷ We collected multiview behavior and utilized a combination of unsupervised clustering and supervised refinement. This allowed us to deconstruct the organizational structure into high-dimensional postures, which were then transitioned to low-dimensional individual states. We propose an analytical framework where BehaviorAtlas identifies an individual's 3D spatial postures (layer I). The evolving postures over time form distinct movements (layer II). Based on their biological features, similar types of movements constitute clusters (layer III). The transitions among these movements or clusters form behavioral patterns based on varying durations, frequencies of occurrence, and transition probabilities (layer IV). Different behaviors and their patterns constitute individual patterns under a particular condition (layer V). We present this perspective, which aligns with the previous viewpoints^{2,107} and underscores the importance of combining unsupervised and supervised machine learning as well as integrates multidimensional data with biological significance. HBAF has the potential to guarantee properties such as

pleiotropy, persistence, scalability, generalizability, and valence when it comes to understanding behaviors. Furthermore, this framework enables interpretation of the underlying biological significance of variations in these behaviors. Additionally, HBAF could be utilized to comprehend how neural circuits integrate internal and external cues to generate behavioral states.^{35,108}

Behavior reflects the brain state externally,^{35,108} and exploration is an innate behavior that does not rely on external cues.^{51–53,109} In mice, sniffing during exploration is biologically significant for sensory input,^{110,111} neuronal processing,¹¹² and adaptative behavior.^{113,114} Mice rely on their sense of smell or touch to perceive their surroundings,^{59,115,116} particularly under conditions of poor light.^{117–119} We propose that exploration, especially sniffing, may represent a conscious state for mice in their spontaneous activity, and the reliance on scent-based perception explains why sniffing is crucial in their movement transition. Despite exhibiting various behavioral abnormalities under AS, sniffing remains fundamental, indicating that the effects of AS may be reversible. However, if this type of stress persists and leads to more severe negative emotional status or the development of psychiatric disorders, then the significance of sniffing in their behavior pattern may alter.

Using HBAF for analyzing postures to behavioral patterns aids comprehension of animal behavior

Here, we outline the potential applications of HBAF. Initially, it can aid in rapidly and accurately evaluating animal behavioral states by calculating and comparing the sniffing-to-grooming ratio of different groups, with a particular focus on the initial 10-min data in corners of the open field arena. By examining movement transition frequencies, conducting principal-component analysis, and performing sniffing ratio analysis, it is possible to enable high-throughput drug screening, evaluate intervention efficacy, and determine the success of newly established animal models. Subsequently, through analysis of high-dimensional data like posture and movements, such as gesture analysis of specific movements without external measurements, it facilitates rapid identification and quantitative measurement of various diseases, such as Parkinson's disease,¹²⁰ autism,^{31,43} colitis,¹²¹ and ankylosing spondylitis.¹²² Looking to the future, by creating a comprehensive behavior atlas of normal animal or disease models during the lifespan, it may be possible to develop an early disease prediction model based on behavioral phenotypes.

Figure 4. Dynamics of spontaneous behavior in mice over 60 min

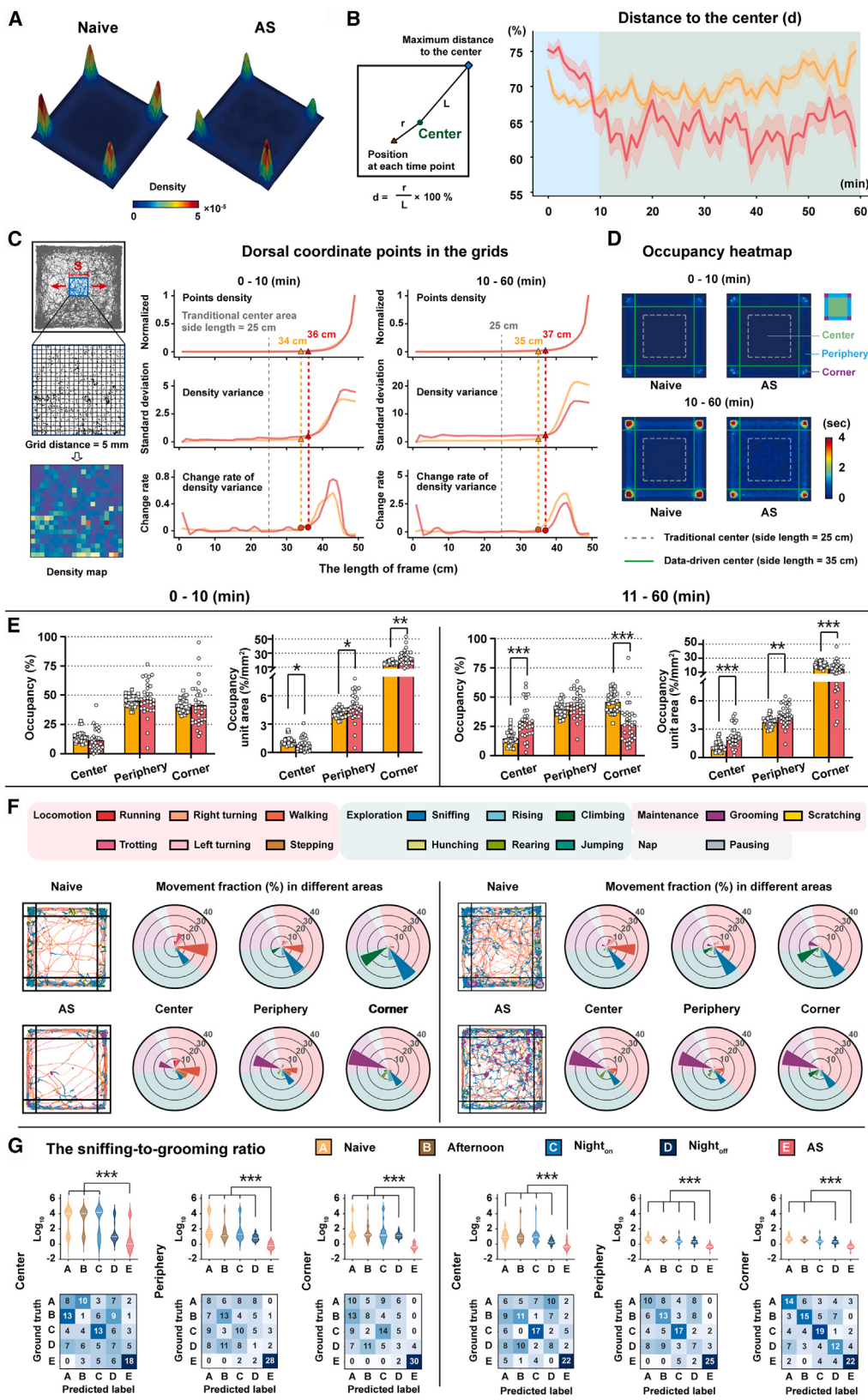
(A) Temporal occurrence of each movement. Data are presented as the mean normalized values over the time course of each movement. Each small row indicated one mouse. The correlation between the movement occurrence probabilities and experiment execution time was examined using Pearson correlation coefficient analysis. Yellow: the naive group, $n = 15$ for each sex. Red: the AS group, $n = 16$ for each sex. r: Pearson correlation coefficient. Red number: increase over time. Blue number: decrease over time. * $p < 0.05$, ** $p < 0.01$, *** $p < 0.001$.

(B) The travel distance was measured each minute throughout the experiment, with the total locomotion distance shown on the right. Data are presented as mean \pm SEM. Normality was tested by a Shapiro-Wilk test (statistic = 0.984, $p = 0.612$, was normally distributed). two-way ANOVA was performed to examine the differences in the total distance: $F_{\text{interaction}}(1, 58) = 1.14, p = 0.2896$; $F_{\text{sex}}(1, 58) = 3.50, p = 0.0664$; $F_{\text{group}}(1, 58) = 16.7, p = 0.0001$, with Bonferroni multiple comparisons. * $p < 0.05$, ** $p < 0.01$, *** $p < 0.001$.

(C) The similarities of behavioral repertoires across different pairwise time intervals within the mouse population were analyzed. Columns and rows represent several corresponding 5-min time blocks within a 60-min experiment, and each cell in the heatmap represents the average similarity of behavioral repertoires at the population level when comparing pairwise time blocks. Closer correlation distances shown in red indicate higher similarities.

(D) Changes in cluster proportion between different time intervals. The changing rates of movement cluster proportion were calculated by comparing the average cluster fractions of the later time block to those of the former.

See also Figure S7.



(legend on next page)

HBAF enables the rediscovery of spontaneous behaviors following AS across time

The open field test is commonly employed for assessing anxiety-like levels of mice following stress.^{123,124} Conventionally, the test is carried out for 10–15 min^{97,125}; a decrease in the time spent in the central area is frequently interpreted as an indicator of increased anxiety-like behavior.^{97,126,127} The current study shows that the spatial preference of mice subjected to AS in the open field test exhibits a dimorphic phenotype that evolves over time. Initially, the AS mice showed a decrease in time spent in the central area during the first 10 min, consistent with previous findings.^{97,98} But they then went on to spend more time in the central area over the following 50 min. This suggests that caution is warranted when interpreting previous studies on anxiety-like behavior, which are often based on only 10 min of spontaneous behavior. Additionally, the AS mice exhibit a notable decrease in exploration and a significant increase in maintenance. It raises the question of whether the increased grooming and scratching represent a conscious response to anxiety-like emotional status in the brain or whether it could be a potential active manifestation of behavior to alleviate anxiety.¹²⁸ Interestingly, the AS mice also showed postural abnormalities, such as a reduction in the height of their dorsal points during movement and a tendency to hunch their bodies while exploring, which closely resemble manifestations seen in humans during states of anxiety,¹²⁹ which may contribute to identifying anxiety-like behavior. Based on these findings, we proposed that a decrease in the sniffing-to-grooming ratio may serve as an indicator of heightened anxiety levels. Further experiments are necessary to confirm these hypotheses.

Generating a comprehensive and informative dataset regarding the spontaneous behavior atlas in mice of both sexes using HBAF

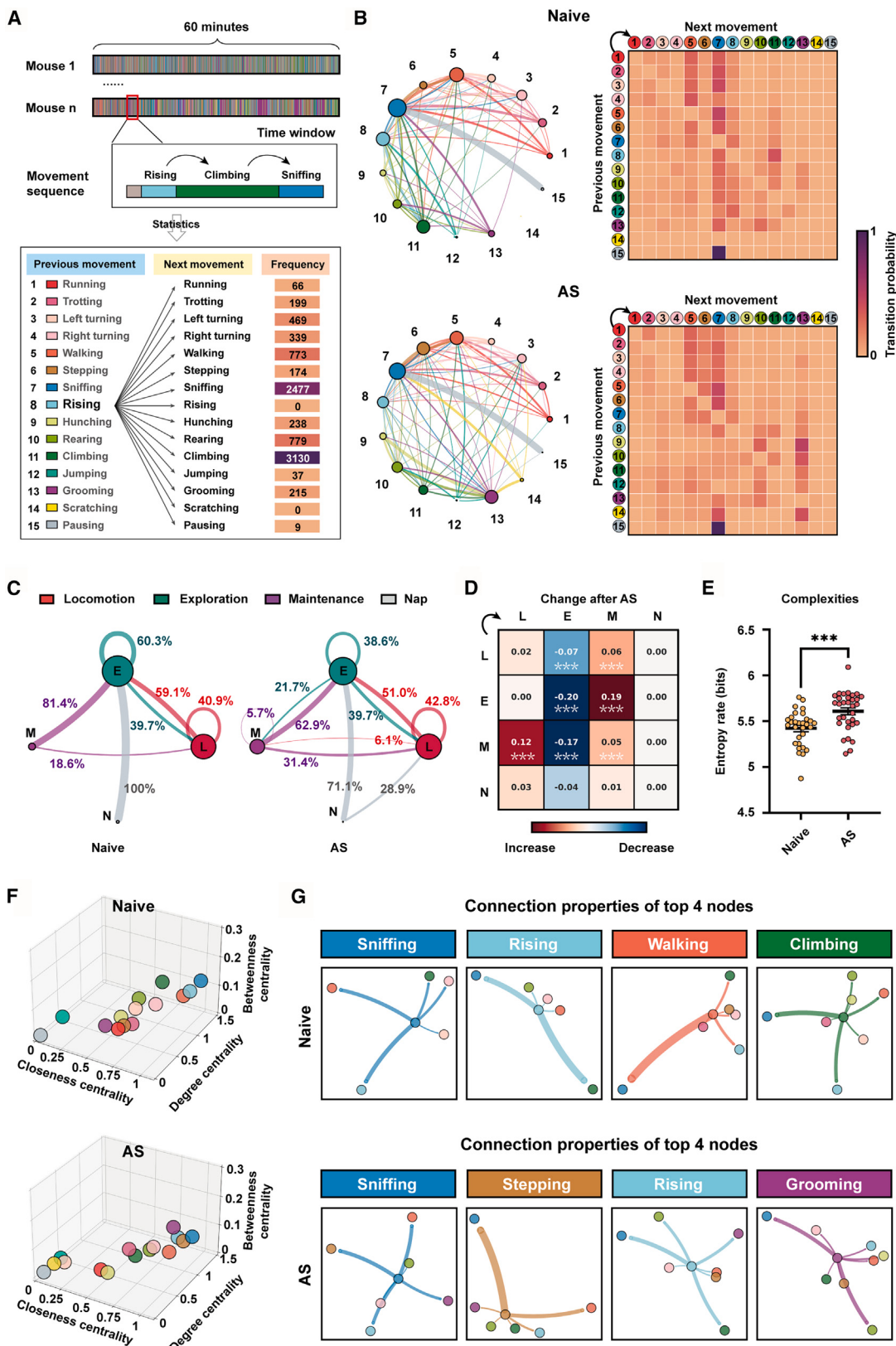
There is an ongoing debate regarding whether behavioral testing in rodents should be conducted during their active or resting phase.^{130,131} Mice are more active in their home cage at night^{46,47,132} or in dark open field arenas.¹³³ Our find-

ings revealed that mice exhibited highly similar locomotion and exploration during the initial 15 min after entering the arena, consistent with previous findings.^{43,134} Subsequently, mice exhibit more self-attentive movements, such as grooming, which is also considered a natural bodycare behavior in low-stress situations¹⁸ and indicative of stress termination or habituation.⁵⁰ Furthermore, our results demonstrate that mice exhibit increased activity levels during the lightless phase of the day, which is marked by greater movement transitions rather than longer travel distances.¹³⁵ In addition, light has a rapid influence on animal physiology and behavior during the dark phase,¹³⁶ including inhibiting motor activity and reducing melatonin levels.¹³⁷ In naturalistic situations, grooming is thought to be a de-arousal process.^{49,50} Our study confirmed that grooming and pausing were notably increased in mice during the illuminated night phase. These findings imply that mice are more alert at night and experience lower stress levels. Therefore, the impact of light on behavior should be considered when conducting experiments during nocturnal hours. These findings provide a valuable resource for investigators aiming to optimize their behavioral experimental design. It emphasizes the importance of considering the time of day for conducting experiments and the inclusion of both male and female mice.

In brief, while our approaches show promise in creating improved animal models for various brain diseases and expediting interventions and drug discovery, the current behavioral assessment systems pose a significant obstacle to gaining deeper insights into brain disorders. We believe that our proposed behavior pattern analysis framework represents an exciting opportunity in this field. Notably, this framework utilizes high-dimensional behavioral data from natural animal conditions, allowing for the incorporation of posture information across any time and space dimensions. Our findings indicate that the unbiased identification of concealed behavioral phenotypes may help address this bottleneck and advance the field toward impartial assessment approaches for behaviors.

Figure 5. Spatial preference and spatial activity pattern in the open field arena

- (A) Density map of the spatial distribution of dorsal points in 60-min open field activity.
 - (B) The average distance ratio to the center point (d) was calculated per minute. Data are presented as mean \pm SEM. Yellow: naive group. Red: AS group.
 - (C) Calculating the density by grids and identifying the region-dividing boundary (see also Figure S8). Left: the calculation of grid density. Right: the change in density and density variance and the derivation of density variance as the central frame expanded. The point where the rising rate of density variance exceeds the 10% peak is shown as the boundary of the central area. This expanding boundary line divided the open field arena into three distinct regions. The gray, yellow, and red dashed lines indicate the side length of the central region of traditionally defined, naive, and AS mice in different periods, respectively.
 - (D) Diagrams illustrate the division of the open field arena into the center, the periphery, and the corner region using the newly proposed method (green solid line; side length of the center is 35 cm) and the traditional method (gray dashed line, with a center side length of 25 cm). The heatmap displays occupancy time in the open field arena. Red: longer residence time. Blue: shorter residence time.
 - (E) The occupancy and the unit area occupancy in the center, periphery, and corner during the first 10 min (left) and the subsequent 50 min (right). A Mann-Whitney test was performed with Bonferroni-Dunn multiple comparisons. * $p < 0.05$, ** $p < 0.01$, *** $p < 0.001$.
 - (F) The fraction of movements and clusters in the center, periphery, and corner for the naive and AS groups during the first 10 min (left) and the subsequent 50 min (right). The larger size of the segment area indicates a higher movement fraction in that region.
 - (G) The sniffing-to-grooming ratio during movement in various groups within specific time intervals and areas (top) along with the classification accuracy of a random forest classifier trained using the respective sniffing-to-grooming ratios (bottom). Numbers in the heatmap indicated the number of mice. The sniffing-to-grooming ratio values were transformed logarithmically, and differences were assessed using a Kruskal-Wallis test with Dunn's multiple comparisons. * $p < 0.05$, ** $p < 0.01$, *** $p < 0.001$.
- The occupancy data shown in (B) and (E) are presented as mean \pm SEM, and movement fractions in different regions shown in (F) are presented as mean. The sniffing-to-grooming ratio in (G) is displayed using a logarithmic violin plot. The source data and statistical information are provided in Table S3.



(legend on next page)

Limitations of the study

In the multiple-view animal motion capture system, we used a transparent enclosure, which is different from the traditional opaque open field assay. Additionally, due to the high similarities in the kinetics features of postures, such as distinguishing between pausing and low-displacement sniffing, as well as climbing and rearing, some movements were subsequently corrected using specific rules. Furthermore, the recording setup varied based on lighting conditions, employing the red, green, and blue (RGB) color model during bright phases and the infrared model in dark phases. This variation may have introduced some bias in the multipoint tracking task during the initial step of the behavior analysis system. While we did not explore the concept of generating “virtual mice” in this study, we believe that applying deep reinforcement learning to train mouse models¹³⁸ based on the multidimensional behavioral data collected from HBAF holds considerable theoretical and practical significance.

RESOURCE AVAILABILITY

Lead contact

Requests for further information, resources, and reagents should be directed to the lead contact, Feng Wang (feng.wang@siat.ac.cn).

Materials availability

This study did not generate new unique reagents.

Data and code availability

- The data supporting the current study’s findings are available at Zenodo (<https://zenodo.org/records/10037411>) and are publicly available as of the date of publication. Original videos will be shared by the **lead contact** upon request.
- All original code has been deposited at GitHub (<https://github.com/Feng-Wang-Research-Group/The-hierarchical-behavioral-analysis-framework>) and is publicly available as of the date of publication. Information on behavioral decomposition software (BehaviorAtlas) can be found at <https://bayonesci.com/behavioratlas>.
- Any additional information required to reanalyze the data reported in this paper is available from the **lead contact** upon request.

ACKNOWLEDGMENTS

This work was supported by the National Science and Technology Innovation 2030-Major Project of China (grant 2022ZD0208300 to F.W.), the National Natural Science Foundation of China (grant 32371062 to F.W., 31630031 and

31930047 to L.W., Research Fund for International Senior Scientists grant T2250710685, and NSFC-Guangdong Joint Fund grant U20A6005), the Guangdong Provincial Key Laboratory of Brain Connectome and Behavior (grant 2023B1212060055 to L.W.), the Guangdong Basic and Applied Basic Research Foundation (grant 2022A1515110120), the Shenzhen Key Basic Research Project (grant JCYJ20220818100805013 to F.W.), and financial support for the Outstanding Talents Training Fund in Shenzhen (to L.W.). We extend our heartfelt appreciation to Prof. Wei Zhao for supplying the data analysis workstation and to Prof. Helmut Kettenmann, Prof. Bai Lu, Prof. Liming Tan, Prof. Minghu Han, Prof. Ji Hu, and Prof. Chaoran Ren for their helpful comments and thoughtful suggestions on the manuscript. We would like to express our sincere gratitude to the members of Feng Wang’s lab for their helpful comments and kind suggestions regarding the manuscript.

AUTHOR CONTRIBUTIONS

F.W. designed the experiments. J.Y., Y.X., K.H., and X.W. conducted the experiments and generated the training dataset for multiple-point tracing of a mouse. J.Y. performed data analyses and produced figures. J.Y. wrote the first draft of the manuscript. L.W. and F.W. revised the manuscript and supported all aspects of this project.

DECLARATION OF INTERESTS

The authors declare no competing interests.

STAR METHODS

Detailed methods are provided in the online version of this paper and include the following:

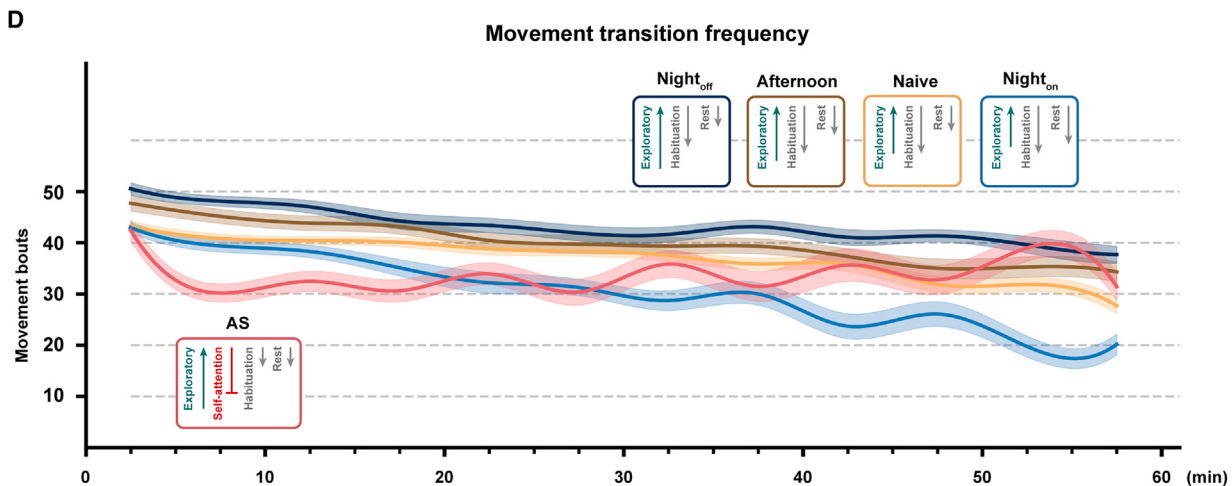
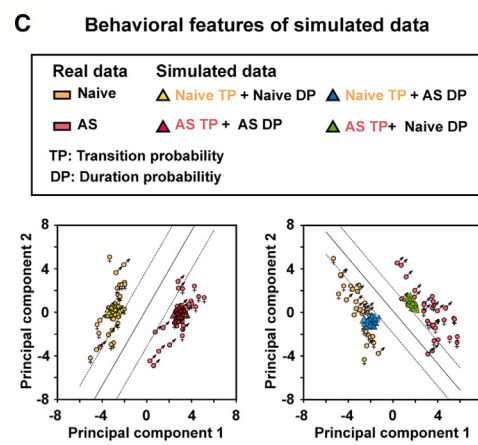
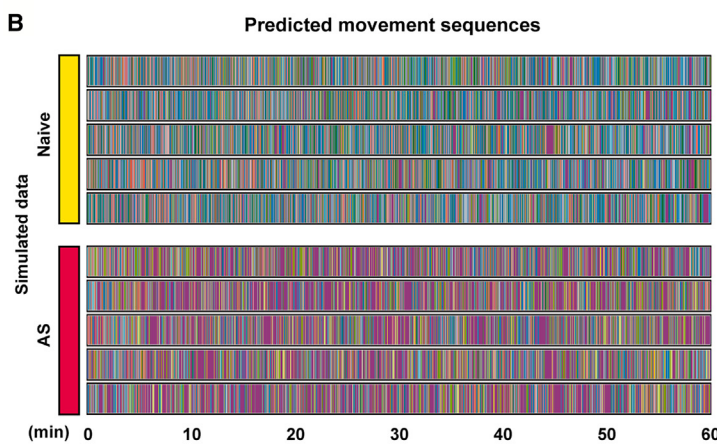
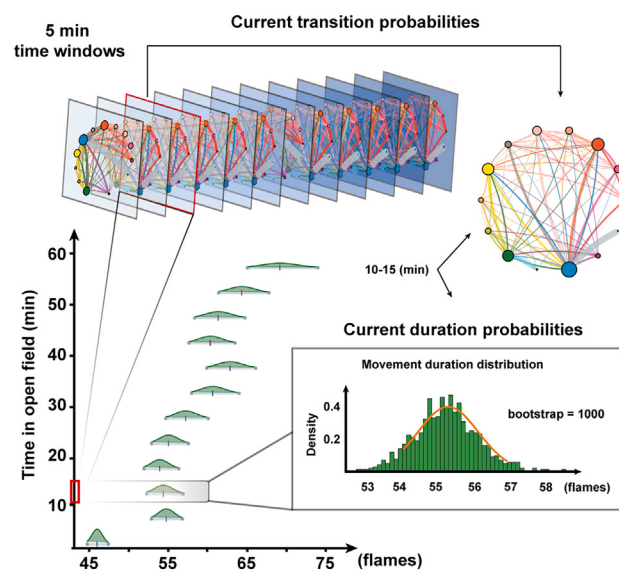
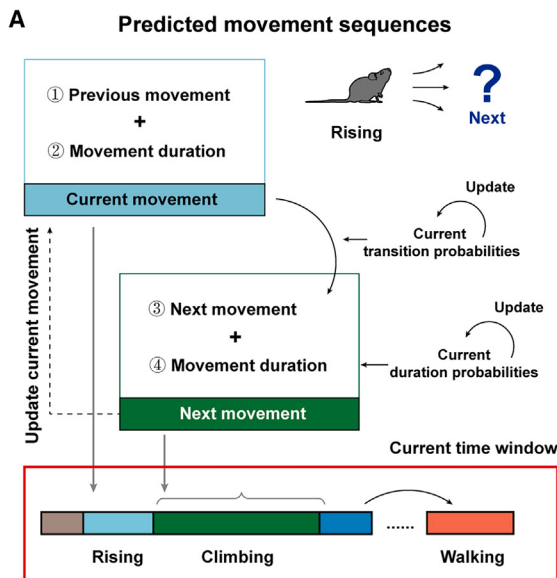
- **KEY RESOURCES TABLE**
- **EXPERIMENTAL MODEL AND STUDY PARTICIPANT DETAILS**
 - Mice
- **METHOD DETAILS**
 - Apparatus
 - Experimental design and randomization
 - Acute restraint stress model¹³⁹
 - Spontaneous behavioral procedure
 - Behavioral data processing
- **QUANTIFICATION AND STATISTICAL ANALYSIS**
 - Statistical analysis

SUPPLEMENTAL INFORMATION

Supplemental information can be found online at <https://doi.org/10.1016/j.celrep.2025.115239>.

Figure 6. Movement transition probability-driven behavior pattern

- (A) Schematic of estimating the probability of one movement turning to another.
- (B) Movement transition probabilities under various experimental conditions. Each movement bout is represented as a state, where the circle size represents the number of movement bouts, with larger circles indicating higher occurrence frequency. The colored arrow indicates transitions from this movement to others (left), and their sizes are scaled based on the transition probabilities between movements. Only transition probabilities exceeding 0.05 are shown on the state transition map (right), with darker shades in the transition matrix heatmap indicating higher transition probabilities (see also Figure S9A).
- (C) Clusters transition probabilities, with clusters represented by labels such as L (locomotion), E (exploration), M (maintenance), and N (nap), where the circle size represents the number of cluster bouts, with larger circles indicating higher occurrence frequency. Thicker connecting lines between two nodes indicate higher transition probabilities.
- (D) The heatmap showed the average difference in cluster transition probabilities, revealing changes in the AS group compared to the naive group, with red indicating increased transition probabilities in AS, and blue indicating decreased transitions. A permutation test with 10,000 random shuffles was used to evaluate the average differences in the transition probabilities between the two groups (see also Figure S9B).
- (E) First-order entropy rates of movement transitions. Each dot represents a mouse. An unpaired two-tailed Student’s t-test with Welch’s correction ($p = 0.0006$) was used. The data are presented as mean \pm SEM.
- (F) Centralities of each movement in the transition network. Top: the naive group. Bottom: the AS group. See also Figure S9C.
- (G) Connection properties of the top 4 nodes in the movement transition process. Top: the naive group. Bottom: the AS group. The larger distance with a thicker connection line between two nodes indicates higher transition probabilities. Only transition probabilities >0.05 are shown (see also Figure S9D).



(legend on next page)

Received: August 21, 2024
 Revised: November 19, 2024
 Accepted: January 7, 2025
 Published: February 1, 2025

REFERENCES

- Holloway, A.L., and Lerner, T.N. (2024). Hidden variables in stress neurobiology research. *Trends Neurosci.* 47, 9–17. <https://doi.org/10.1016/j.tins.2023.10.006>.
- Anderson, D.J., and Perona, P. (2014). Toward a science of computational ethology. *Neuron* 84, 18–31. <https://doi.org/10.1016/j.neuron.2014.09.005>.
- von Ziegler, L., Sturman, O., and Bohacek, J. (2021). Big behavior: challenges and opportunities in a new era of deep behavior profiling. *Neuro-psychopharmacology* 46, 33–44. <https://doi.org/10.1038/s41386-020-0751-7>.
- Datta, S.R., Anderson, D.J., Branson, K., Perona, P., and Leifer, A. (2019). Computational Neuroethology: A Call to Action. *Neuron* 104, 11–24. <https://doi.org/10.1016/j.neuron.2019.09.038>.
- Gomez-Marin, A., Paton, J.J., Kampff, A.R., Costa, R.M., and Mainen, Z.F. (2014). Big behavioral data: psychology, ethology and the foundations of neuroscience. *Nat. Neurosci.* 17, 1455–1462. <https://doi.org/10.1038/nn.3812>.
- Marshall, J.D., Aldarondo, D.E., Dunn, T.W., Wang, W.L., Berman, G.J., and Ölveczky, B.P. (2021). Continuous Whole-Body 3D Kinematic Recordings across the Rodent Behavioral Repertoire. *Neuron* 109, 420–437.e8. <https://doi.org/10.1016/j.neuron.2020.11.016>.
- Goodwin, N.L., Choong, J.J., Hwang, S., Pitts, K., Bloom, L., Islam, A., Zhang, Y.Y., Szelenyi, E.R., Tong, X., Newman, E.L., et al. (2024). Simple Behavioral Analysis (SimBA) as a platform for explainable machine learning in behavioral neuroscience. *Nat. Neurosci.* 27, 1411–1424. <https://doi.org/10.1038/s41593-024-01649-9>.
- tinbergen, N. (1951). *The Study of Instinct* (Clarendon Press/Oxford University Press).
- Berridge, K.C., Fentress, J.C., and Parr, H. (1987). Natural syntax rules control action sequence of rats. *Behav. Brain Res.* 23, 59–68. [https://doi.org/10.1016/0166-4328\(87\)90242-7](https://doi.org/10.1016/0166-4328(87)90242-7).
- Gallistel, C.R. (1981). Précis of Gallistel's *The organization of action: A new synthesis*. *Behav. Brain Sci.* 4, 609–619.
- Fentress, J.C., and Stilwell, F.P. (1973). Grammar of a movement sequence in inbred mice. *Nature* 244, 52–53. <https://doi.org/10.1038/244052a0>.
- Mazzucato, L. (2022). Neural mechanisms underlying the temporal organization of naturalistic animal behavior. *Elife* 11, e76577. <https://doi.org/10.7554/eLife.76577>.
- Wiltschko, A.B., Johnson, M.J., Iurilli, G., Peterson, R.E., Katon, J.M., Pashkovski, S.L., Abraira, V.E., Adams, R.P., and Datta, S.R. (2015). Mapping Sub-Second Structure in Mouse Behavior. *Neuron* 88, 1121–1135. <https://doi.org/10.1016/j.neuron.2015.11.031>.
- Flavell, S.W., Raizen, D.M., and You, Y.J. (2020). Behavioral States. *Genetics* 216, 315–332. <https://doi.org/10.1534/genetics.120.303539>.
- Flavell, S.W., Gogolla, N., Lovett-Barron, M., and Zelikowsky, M. (2022). The emergence and influence of internal states. *Neuron* 110, 2545–2570. <https://doi.org/10.1016/j.neuron.2022.04.030>.
- Pillai, A.S., and Jirsa, V.K. (2017). Symmetry Breaking in Space-Time Hierarchies Shapes Brain Dynamics and Behavior. *Neuron* 94, 1010–1026. <https://doi.org/10.1016/j.neuron.2017.05.013>.
- Markowitz, J.E., Gillis, W.F., Beron, C.C., Neufeld, S.Q., Robertson, K., Bhagat, N.D., Peterson, R.E., Peterson, E., Hyun, M., Linderman, S.W., et al. (2018). The Striatum Organizes 3D Behavior via Moment-to-Moment Action Selection. *Cell* 174, 44–58.e17. <https://doi.org/10.1016/j.cell.2018.04.019>.
- Kalueff, A.V., and Tuohimaa, P. (2004). Grooming analysis algorithm for neurobehavioural stress research. *Brain Res. Brain Res. Protoc.* 13, 151–158. <https://doi.org/10.1016/j.brainresprot.2004.04.002>.
- Nath, T., Mathis, A., Chen, A.C., Patel, A., Bethge, M., and Mathis, M.W. (2019). Using DeepLabCut for 3D markerless pose estimation across species and behaviors. *Nat. Protoc.* 14, 2152–2176. <https://doi.org/10.1038/s41596-019-0176-0>.
- Pereira, T.D., Aldarondo, D.E., Willmore, L., Kislin, M., Wang, S.S.H., Murthy, M., and Shaevitz, J.W. (2019). Fast animal pose estimation using deep neural networks. *Nat. Methods* 16, 117–125. <https://doi.org/10.1038/s41592-018-0234-5>.
- Pereira, T.D., Tabris, N., Matsliah, A., Turner, D.M., Li, J., Ravindranath, S., Papadoyannis, E.S., Normand, E., Deutsch, D.S., Wang, Z.Y., et al. (2022). SLEAP: A deep learning system for multi-animal pose tracking. *Nat. Methods* 19, 486–495. <https://doi.org/10.1038/s41592-022-01426-1>.
- Mathis, A., Mamidanna, P., Cury, K.M., Abe, T., Murthy, V.N., Mathis, M.W., and Bethge, M. (2018). DeepLabCut: markerless pose estimation of user-defined body parts with deep learning. *Nat. Neurosci.* 21, 1281–1289. <https://doi.org/10.1038/s41593-018-0209-y>.
- Graving, J.M., Chae, D., Naik, H., Li, L., Koger, B., Costelloe, B.R., and Couzin, I.D. (2019). DeepPoseKit, a software toolkit for fast and robust animal pose estimation using deep learning. *Elife* 8, e47994. <https://doi.org/10.7554/elife.47994>.
- Dunn, T.W., Marshall, J.D., Severson, K.S., Aldarondo, D.E., Hildebrand, D.G.C., Chettih, S.N., Wang, W.L., Gellis, A.J., Carlson, D.E., Aronov, D., et al. (2021). Geometric deep learning enables 3D kinematic profiling across species and environments. *Nat. Methods* 18, 564–573. <https://doi.org/10.1038/s41592-021-01106-6>.
- Karashchuk, P., Rupp, K.L., Dickinson, E.S., Walling-Bell, S., Sanders, E., Azim, E., Brunton, B.W., and Tuthill, J.C. (2021). Anipose: A toolkit for robust markerless 3D pose estimation. *Cell Rep.* 36, 109730. <https://doi.org/10.1016/j.celrep.2021.109730>.
- Weinreb, C., Pearl, J., Lin, S., Osman, M.A.M., Zhang, L., Annapragada, S., Conlin, E., Hoffman, R., Makowska, S., Gillis, W.F., et al. (2023). Key-point-MoSeq: parsing behavior by linking point tracking to pose dynamics. Preprint at bioRxiv. <https://doi.org/10.1101/2023.03.16.532307>.

Figure 7. Prediction of behavior pattern

- (A) The dynamic transition and duration probability together constitute the phase-specific behavior pattern, which was used to generate the simulated movement sequence. The next movement was extrapolated based on the dynamic movement transition probabilities, and the occurring movement's duration was inferred from the corresponding movement duration probabilities.
- (B) Ethograms of simulated data based on the naive and AS groups for 5 representative mice.
- (C) PCA of behavioral features between real data and simulated data. The simulated data (left) were generated by the match probabilities, and those on the right were generated by interchanged movement duration probabilities. TP, transition probability; DP, duration probability. Yellow: data from the naive group. Light yellow: simulated data using TP and DP data, both from naive mice. Red: data from the AS group. Deep red: simulated data using TP and DP data, both from the AS group. Blue: simulated data using TP data from naive mice and DP data from AS mice. Green: simulated data using TP data from AS mice and DP data from naive mice. See also [Figures S10A–S10C](#).
- (D) The movement transition frequencies under various experimental conditions were determined by calculating movement bouts that occurred every 5 min (see also [Figure S10D](#)).

27. Hsu, A.I., and Yttri, E.A. (2021). B-SOI_D, an open-source unsupervised algorithm for identification and fast prediction of behaviors. *Nat. Commun.* 12, 5188. <https://doi.org/10.1038/s41467-021-25420-x>.
28. Segalin, C., Williams, J., Karigo, T., Hui, M., Zelikowsky, M., Sun, J.J., Perona, P., Anderson, D.J., and Kennedy, A. (2021). The Mouse Action Recognition System (MARS) software pipeline for automated analysis of social behaviors in mice. *Elife* 10, e63720. <https://doi.org/10.7554/elife.63720>.
29. Luxem, K., Mocellin, P., Fuhrmann, F., Kürsch, J., Miller, S.R., Palop, J.J., Remy, S., and Bauer, P. (2022). Identifying behavioral structure from deep variational embeddings of animal motion. *Commun. Biol.* 5, 1267. <https://doi.org/10.1038/s42003-022-04080-7>.
30. Berman, G.J., Choi, D.M., Bialek, W., and Shaevitz, J.W. (2014). Mapping the stereotyped behaviour of freely moving fruit flies. *J. R. Soc. Interface* 11, 20140672. <https://doi.org/10.1098/rsif.2014.0672>.
31. Huang, K., Han, Y., Chen, K., Pan, H., Zhao, G., Yi, W., Li, X., Liu, S., Wei, P., and Wang, L. (2021). A hierarchical 3D-motion learning framework for animal spontaneous behavior mapping. *Nat. Commun.* 12, 2784. <https://doi.org/10.1038/s41467-021-22970-y>.
32. Ye, S., Filippova, A., Lauer, J., Schneider, S., Vidal, M., Qiu, T., Mathis, A., and Mathis, M.W. (2024). SuperAnimal pretrained pose estimation models for behavioral analysis. *Nat. Commun.* 15, 5165. <https://doi.org/10.1038/s41467-024-48792-2>.
33. McGinley, M.J., Vinck, M., Reimer, J., Batista-Brito, R., Zagha, E., Cadwell, C.R., Tolias, A.S., Cardin, J.A., and McCormick, D.A. (2015). Waking State: Rapid Variations Modulate Neural and Behavioral Responses. *Neuron* 87, 1143–1161. <https://doi.org/10.1016/j.neuron.2015.09.012>.
34. Stringer, C., Pachitariu, M., Steinmetz, N., Reddy, C.B., Carandini, M., and Harris, K.D. (2019). Spontaneous behaviors drive multidimensional, brainwide activity. *Science* 364, 255. <https://doi.org/10.1126/science.aav7893>.
35. Miller, C.T., Gire, D., Hoke, K., Huk, A.C., Kelley, D., Leopold, D.A., Smear, M.C., Theunissen, F., Yartsev, M., and Niell, C.M. (2022). Natural behavior is the language of the brain. *Curr. Biol.* 32, R482–R493. <https://doi.org/10.1016/j.cub.2022.03.031>.
36. Puscsian, A., and Knapska, E. (2022). Blueprints for measuring natural behavior. *iScience* 25, 104635. <https://doi.org/10.1016/j.isci.2022.104635>.
37. Kennedy, A. (2022). The what, how, and why of naturalistic behavior. *Curr. Opin. Neurobiol.* 74, 102549. <https://doi.org/10.1016/j.conb.2022.102549>.
38. Smith, K. (2023). Lab mice go wild: making experiments more natural in order to decode the brain. *Nature* 618, 448–450. <https://doi.org/10.1038/d41586-023-01926-w>.
39. Bohic, M., Pattison, L.A., Jhumka, Z.A., Rossi, H., Thackray, J.K., Ricci, M., Mossazghi, N., Foster, W., Ogundare, S., Twomey, C.R., et al. (2023). Mapping the neuroethological signatures of pain, analgesia, and recovery in mice. *Neuron* 111, 2811–2830.e8. <https://doi.org/10.1016/j.neuron.2023.06.008>.
40. Xie, Z., Zhang, X., Zhao, M., Huo, L., Huang, M., Li, D., Zhang, S., Cheng, X., Gu, H., Zhang, C., et al. (2022). The gut-to-brain axis for toxin-induced defensive responses. *Cell* 185, 4298–4316.e21. <https://doi.org/10.1016/j.cell.2022.10.001>.
41. Gschwind, T., Zeine, A., Raikov, I., Markowitz, J.E., Gillis, W.F., Felong, S., Isom, L.L., Datta, S.R., and Soltesz, I. (2023). Hidden behavioral fingerprints in epilepsy. *Neuron* 111, 1440–1452.e5. <https://doi.org/10.1016/j.neuron.2023.02.003>.
42. Weber, R.Z., Mulders, G., Kaiser, J., Tackenberg, C., and Rust, R. (2022). Deep learning-based behavioral profiling of rodent stroke recovery. *BMC Biol.* 20, 232. <https://doi.org/10.1186/s12915-022-01434-9>.
43. Klibaite, U., Kislin, M., Verpeut, J.L., Bergeler, S., Sun, X., Shaevitz, J.W., and Wang, S.S.H. (2022). Deep phenotyping reveals movement phenotypes in mouse neurodevelopmental models. *Mol. Autism.* 13, 12. <https://doi.org/10.1186/s13229-022-00492-8>.
44. Anderson, D.J., and Adolphs, R. (2014). A framework for studying emotions across species. *Cell* 157, 187–200. <https://doi.org/10.1016/j.cell.2014.03.003>.
45. Chen, D., Lou, Q., Song, X.-J., Kang, F., Liu, A., Zheng, C., Li, Y., Wang, D., Qun, S., Zhang, Z., et al. (2024). Microglia govern the extinction of acute stress-induced anxiety-like behaviors in male mice. *Nat. Commun.* 15, 449. <https://doi.org/10.1038/s41467-024-44704-6>.
46. Fuochi, S., Rigamonti, M., Iannello, F., Raspa, M., Scavizzi, F., de Girolamo, P., and D'Angelo, L. (2021). Phenotyping spontaneous locomotor activity in inbred and outbred mouse strains by using Digital Ventilated Cages. *Lab Anim.* 50, 215–223. <https://doi.org/10.1038/s41684-021-00793-0>.
47. Miyazaki, Y., Kobayashi, K., Matsushita, S., Shimizu, N., and Murata, T. (2022). An assessment of the spontaneous locomotor activity of BALB/c mice. *J. Pharmacol. Sci.* 149, 46–52. <https://doi.org/10.1016/j.jphs.2022.03.001>.
48. Bolles, R.C. (1960). Grooming behavior in the rat. *J. Comp. Physiol. Psychol.* 53, 306–310. <https://doi.org/10.1037/h0045421>.
49. Kalueff, A.V., Stewart, A.M., Song, C., Berridge, K.C., Graybiel, A.M., and Fentress, J.C. (2016). Neurobiology of rodent self-grooming and its value for translational neuroscience. *Nat. Rev. Neurosci.* 17, 45–59. <https://doi.org/10.1038/nrn.2015.8>.
50. Spruijt, B.M., van Hooff, J.A., and Gispen, W.H. (1992). Ethology and neurobiology of grooming behavior. *Physiol. Rev.* 72, 825–852. <https://doi.org/10.1152/physrev.1992.72.3.825>.
51. Poli, F., O'Reilly, J.X., Mars, R.B., and Hunnius, S. (2024). Curiosity and the dynamics of optimal exploration. *Trends Cogn. Sci.* 28, 441. <https://doi.org/10.1016/j.tics.2024.02.001>.
52. Modirshanechi, A., Kondrakiewicz, K., Gerstner, W., and Haesler, S. (2023). Curiosity-driven exploration: foundations in neuroscience and computational modeling. *Trends Neurosci.* 46, 1054–1066. <https://doi.org/10.1016/j.tins.2023.10.002>.
53. Hughes, R.N. (1997). Intrinsic exploration in animals: motives and measurement. *Behav. Processes* 41, 213–226. [https://doi.org/10.1016/s0376-6357\(97\)00055-7](https://doi.org/10.1016/s0376-6357(97)00055-7).
54. Greer, J.M., and Capecchi, M.R. (2002). Hoxb8 is required for normal grooming behavior in mice. *Neuron* 33, 23–34. [https://doi.org/10.1016/s0896-6273\(01\)00564-5](https://doi.org/10.1016/s0896-6273(01)00564-5).
55. Klenowski, P.M., Zhao-Shea, R., Freels, T.G., Molas, S., Zinter, M., M'Angale, P., Xiao, C., Martinez-Núñez, L., Thomson, T., and Tapper, A.R. (2023). A neuronal coping mechanism linking stress-induced anxiety to motivation for reward. *Sci. Adv.* 9, eadh9620. <https://doi.org/10.1126/sciadv.adh9620>.
56. Kalueff, A.V., and Tuohimaa, P. (2005). Contrasting grooming phenotypes in three mouse strains markedly different in anxiety and activity (129S1, BALB/c and NMRI). *Behav. Brain Res.* 160, 1–10. <https://doi.org/10.1016/j.bbr.2004.11.010>.
57. Wesson, D.W., Donahou, T.N., Johnson, M.O., and Wachowiak, M. (2008). Sniffing behavior of mice during performance in odor-guided tasks. *Chem. Senses* 33, 581–596. <https://doi.org/10.1093/chemse/bjn029>.
58. Wachowiak, M. (2011). All in a sniff: olfaction as a model for active sensing. *Neuron* 71, 962–973. <https://doi.org/10.1016/j.neuron.2011.08.030>.
59. Deschenes, M., Moore, J., and Kleinfeld, D. (2012). Sniffing and whisking in rodents. *Curr. Opin. Neurobiol.* 22, 243–250. <https://doi.org/10.1016/j.conb.2011.11.013>.
60. Wolfe, J., Mende, C., and Brecht, M. (2011). Social facial touch in rats. *Behav. Neurosci.* 125, 900–910. <https://doi.org/10.1037/a0026165>.
61. Wesson, D.W., Verhagen, J.V., and Wachowiak, M. (2009). Why sniff fast? The relationship between sniff frequency, odor discrimination,

- and receptor neuron activation in the rat. *J. Neurophysiol.* 101, 1089–1102. <https://doi.org/10.1152/jn.90981.2008>.
62. Liu, A., Papale, A.E., Hengenius, J., Patel, K., Ermentrout, B., and Urban, N.N. (2020). Mouse Navigation Strategies for Odor Source Localization. *Front. Neurosci.* 14, 218. <https://doi.org/10.3389/fnins.2020.00218>.
 63. Liao, S.M., and Kleinfeld, D. (2023). A change in behavioral state switches the pattern of motor output that underlies rhythmic head and orofacial movements. *Curr. Biol.* 33, 1951–1966.e6. <https://doi.org/10.1016/j.cub.2023.04.008>.
 64. Wesson, D.W. (2013). Sniffing behavior communicates social hierarchy. *Curr. Biol.* 23, 575–580. <https://doi.org/10.1016/j.cub.2013.02.012>.
 65. Wei, D., Talwar, V., and Lin, D. (2021). Neural circuits of social behaviors: Innate yet flexible. *Neuron* 109, 1600–1620. <https://doi.org/10.1016/j.neuron.2021.02.012>.
 66. Fortes-Marco, L., Lanuza, E., and Martinez-Garcia, F. (2013). Of pheromones and kairomones: what receptors mediate innate emotional responses? *Anat. Rec.* 296, 1346–1363. <https://doi.org/10.1002/ar.22745>.
 67. Wang, Y., Cao, L., Lee, C.Y., Matsuo, T., Wu, K., Asher, G., Tang, L., Saitoh, T., Russell, J., Klewe-Nebenius, D., et al. (2018). Large-scale forward genetics screening identifies Trpa1 as a chemosensor for predator odor-evoked innate fear behaviors. *Nat. Commun.* 9, 2041. <https://doi.org/10.1038/s41467-018-04324-3>.
 68. Kobayakawa, K., Kobayakawa, R., Matsumoto, H., Oka, Y., Imai, T., Ikawa, M., Okabe, M., Ikeda, T., Itohara, S., Kikusui, T., et al. (2007). Innate versus learned odour processing in the mouse olfactory bulb. *Nature* 450, 503–508. <https://doi.org/10.1038/nature06281>.
 69. Wang, H., Wang, Q., Cui, L., Feng, X., Dong, P., Tan, L., Lin, L., Lian, H., Cao, S., Huang, H., et al. (2024). A molecularly defined amygdala-independent tetra-synaptic forebrain-to-hindbrain pathway for odor-driven innate fear and anxiety. *Nat. Neurosci.* 27, 514–526. <https://doi.org/10.1038/s41593-023-01562-7>.
 70. Hirata, Y. (2021). Recurrence plots for characterizing random dynamical systems. *Commun. Nonlinear Sci. Numer. Simulat.* 94, 105552. <https://doi.org/10.1016/j.cnsns.2020.105552>.
 71. Saiari, A., Khodayari, B., and Bostani, M. (2011). Relation between Increasing Spinal Curve and Anxiety. *Procedia - Soc. Behav. Sci.* 30, 2246–2248. <https://doi.org/10.1016/j.sbspro.2011.10.438>.
 72. Li, P., and Yackle, K. (2017). Sighing. *Curr. Biol.* 27, R88–R89. <https://doi.org/10.1016/j.cub.2016.09.006>.
 73. Bartlett, D., Jr. (1971). Origin and regulation of spontaneous deep breaths. *Respir. Physiol.* 12, 230–238. [https://doi.org/10.1016/0034-5687\(71\)90055-7](https://doi.org/10.1016/0034-5687(71)90055-7).
 74. Lang, M., Krátký, J., Shaver, J.H., Jerotijević, D., and Xygalatas, D. (2015). Effects of Anxiety on Spontaneous Ritualized Behavior. *Curr. Biol.* 25, 1892–1897. <https://doi.org/10.1016/j.cub.2015.05.049>.
 75. Li, L., Feng, X., Zhou, Z., Zhang, H., Shi, Q., Lei, Z., Shen, P., Yang, Q., Zhao, B., Chen, S., et al. (2018). Stress Accelerates Defensive Responses to Looming in Mice and Involves a Locus Coeruleus-Superior Colliculus Projection. *Curr. Biol.* 28, 859–871.e5. <https://doi.org/10.1016/j.cub.2018.02.005>.
 76. Fratzl, A., Koltchev, A.M., Vissers, N., Tan, Y.L., Marques-Smith, A., Stempel, A.V., Branco, T., and Hofer, S.B. (2021). Flexible inhibitory control of visually evoked defensive behavior by the ventral lateral geniculate nucleus. *Neuron* 109, 3810–3822.e9. <https://doi.org/10.1016/j.neuron.2021.09.003>.
 77. Spinelli, R.L., Cazuza, R., Sales, A.J., Carolino, R., Franci, J.A., Tajerian, M., and Leite-Panissi, C.R.A. (2024). Acute restraint stress regulates brain DNMT3a and promotes defensive behaviors in male rats. *Neurosci. Lett.* 820, 137589. <https://doi.org/10.1016/j.neulet.2023.137589>.
 78. Begg, D.P., and Woods, S.C. (2013). The endocrinology of food intake. *Nat. Rev. Endocrinol.* 9, 584–597. <https://doi.org/10.1038/nrendo.2013.136>.
 79. Tu, B.X., Wang, L.F., Zhong, X.L., Hu, Z.L., Cao, W.Y., Cui, Y.H., Li, S.J., Zou, G.J., Liu, Y., Zhou, S.F., et al. (2019). Acute restraint stress alters food-foraging behavior in rats: Taking the easier Way while suffered. *Brain Res. Bull.* 149, 184–193. <https://doi.org/10.1016/j.brainresbull.2019.04.021>.
 80. Francois, M., Canal Delgado, I., Shargorodsky, N., Leu, C.S., and Zeltser, L. (2022). Assessing the effects of stress on feeding behaviors in laboratory mice. *Elife* 11, e70271. <https://doi.org/10.7554/elife.70271>.
 81. Zhao, J., Liu, C., Zhang, F., Zheng, Z., Luo, F., Xia, J., Wang, Y., Zhang, Z., Tang, J., Song, Z., et al. (2022). A paraventricular thalamus to central amygdala neural circuit modulates acute stress-induced heightened wakefulness. *Cell Rep.* 41, 111824. <https://doi.org/10.1016/j.celrep.2022.111824>.
 82. Yu, X., Zhao, G., Wang, D., Wang, S., Li, R., Li, A., Wang, H., Nollet, M., Chun, Y.Y., Zhao, T., et al. (2022). A specific circuit in the midbrain detects stress and induces restorative sleep. *Science* 377, 63–72. <https://doi.org/10.1126/science.abn0853>.
 83. Quartermain, D., Stone, E.A., and Charbonneau, G. (1996). Acute stress disrupts risk assessment behavior in mice. *Physiol. Behav.* 59, 937–940. [https://doi.org/10.1016/0031-9384\(95\)02140-x](https://doi.org/10.1016/0031-9384(95)02140-x).
 84. Fuzeis, T., Daviu, N., Wamsteeker Cusulin, J.I., Bonin, R.P., and Bains, J.S. (2016). Hypothalamic CRH neurons orchestrate complex behaviours after stress. *Nat. Commun.* 7, 11937. <https://doi.org/10.1038/ncomms11937>.
 85. Buynitsky, T., and Mostofsky, D.I. (2009). Restraint stress in biobehavioral research: Recent developments. *Neurosci. Biobehav. Rev.* 33, 1089–1098. <https://doi.org/10.1016/j.neubiorev.2009.05.004>.
 86. Sturman, O., Germain, P.L., and Bohacek, J. (2018). Exploratory rearing: a context- and stress-sensitive behavior recorded in the open-field test. *Stress* 21, 443–452. <https://doi.org/10.1080/10253890.2018.1438405>.
 87. Mitler, M.M., Lund, R., Sokolove, P.G., Pittendrigh, C.S., and Dement, W.C. (1977). Sleep and activity rhythms in mice: a description of circadian patterns and unexpected disruptions in sleep. *Brain Res.* 131, 129–145. [https://doi.org/10.1016/0006-8993\(77\)90033-6](https://doi.org/10.1016/0006-8993(77)90033-6).
 88. Richardson, G.S., Moore-Ede, M.C., Czeisler, C.A., and Dement, W.C. (1985). Circadian rhythms of sleep and wakefulness in mice: analysis using long-term automated recording of sleep. *Am. J. Physiol.* 248, R320–R330. <https://doi.org/10.1152/ajpregu.1985.248.3.R320>.
 89. Spiteri, N.J. (1982). Circadian patterning of feeding, drinking and activity during diurnal food access in rats. *Physiol. Behav.* 28, 139–147. [https://doi.org/10.1016/0031-9384\(82\)90115-9](https://doi.org/10.1016/0031-9384(82)90115-9).
 90. Snell, G.D., Fekete, E., Hummel, K.P., and Law, L.W. (1940). The relation of mating, ovulation and the estrous smear in the house mouse to time of day. *Anat. Rec.* 76, 39–54. <https://doi.org/10.1002/ar.1090760105>.
 91. Beach, F.A., and Levinson, G. (1949). Diurnal variations in the mating behavior of male rats. *Proc. Soc. Exp. Biol. Med.* 72, 78–80. <https://doi.org/10.3181/00379727-72-17337>.
 92. Roth, K.A., and Katz, R.J. (1979). Stress, behavioral arousal, and open field activity—a reexamination of emotionality in the rat. *Neurosci. Biobehav. Rev.* 3, 247–263. [https://doi.org/10.1016/0149-7634\(79\)90012-5](https://doi.org/10.1016/0149-7634(79)90012-5).
 93. Souza, A., Carraro Detanico, B., Fernandes Medeiros, L., Oliveira, C.d., Leal Scarabelot, V., Giotti Cioato, S., Caumo, W., and Torres, I.L. (2017). Acute stress disrupts temporal patterns of behavioral and biochemical parameters of rats. *Biol. Rhythms Res.* 49, 521–538. <https://doi.org/10.1080/09291016.2017.1386267>.
 94. Cryan, J.F., and Holmes, A. (2005). The ascent of mouse: advances in modelling human depression and anxiety. *Nat. Rev. Drug Discov.* 4, 775–790. <https://doi.org/10.1038/nrd1825>.
 95. Shin, L.M., and Liberzon, I. (2010). The neurocircuitry of fear, stress, and anxiety disorders. *Neuropsychopharmacology* 35, 169–191. <https://doi.org/10.1038/npp.2009.83>.

96. Nestler, E.J., and Hyman, S.E. (2010). Animal models of neuropsychiatric disorders. *Nat. Neurosci.* 13, 1161–1169. <https://doi.org/10.1038/nn.2647>.
97. Seibenbener, M.L., and Wooten, M.C. (2015). Use of the Open Field Maze to measure locomotor and anxiety-like behavior in mice. *J. Vis. Exp.* 6, e52434. <https://doi.org/10.3791/52434>.
98. Kraeuter, A.K., Guest, P.C., and Sarnyai, Z. (2019). The Open Field Test for Measuring Locomotor Activity and Anxiety-Like Behavior. *Methods Mol. Biol.* 1916, 99–103. https://doi.org/10.1007/978-1-4939-8994-2_9.
99. Fonio, E., Golani, I., and Benjamini, Y. (2012). Measuring behavior of animal models: faults and remedies. *Nat. Methods* 9, 1167–1170. <https://doi.org/10.1038/nmeth.2252>.
100. Snyder, C.N., Brown, A.R., and Buffalari, D. (2021). Similar tests of anxiety-like behavior yield different results: comparison of the open field and free exploratory rodent procedures. *Physiol. Behav.* 230, 113246. <https://doi.org/10.1016/j.physbeh.2020.113246>.
101. Calatayud, F., Belzung, C., and Aubert, A. (2004). Ethological validation and the assessment of anxiety-like behaviours: methodological comparison of classical analyses and structural approaches. *Behav. Processes* 67, 195–206. <https://doi.org/10.1016/j.beproc.2004.04.002>.
102. Simon, P., Dupuis, R., and Costentin, J. (1994). Thigmotaxis as an index of anxiety in mice. Influence of dopaminergic transmissions. *Behav. Brain Res.* 61, 59–64. [https://doi.org/10.1016/0166-4328\(94\)90008-6](https://doi.org/10.1016/0166-4328(94)90008-6).
103. Makino, J., Kato, K., and Maes, F.W. (1991). Temporal structure of open field behavior in inbred strains of mice. *Jpn. Psychol. Res.* 33, 145–152. <https://doi.org/10.4992/psycholres1954.33.145>.
104. Reddy, G., Desban, L., Tanaka, H., Roussel, J., Mirat, O., and Wyart, C. (2022). A lexical approach for identifying behavioural action sequences. *PLoS Comput. Biol.* 18, e1009672. <https://doi.org/10.1371/journal.pcbi.1009672>.
105. VanHook, A.M. (2010). Behavioral Fingerprinting. *Sci. Signal.* 3, ec22. <https://doi.org/10.1126/scisignal.3105ec22>.
106. Branson, K., Robie, A.A., Bender, J., Perona, P., and Dickinson, M.H. (2009). High-throughput ethomics in large groups of *Drosophila*. *Nat. Methods* 6, 451–457. <https://doi.org/10.1038/nmeth.1328>.
107. Gris, K.V., Couto, J.P., and Gris, D. (2017). Supervised and Unsupervised Learning Technology in the Study of Rodent Behavior. *Front. Behav. Neurosci.* 11, 141. <https://doi.org/10.3389/fnbeh.2017.00141>.
108. Pereira, T.D., Shaevitz, J.W., and Murthy, M. (2020). Quantifying behavior to understand the brain. *Nat. Neurosci.* 23, 1537–1549. <https://doi.org/10.1038/s41593-020-00734-z>.
109. Berlyne, D.E. (1966). Curiosity and Exploration. *Science* 153, 25–33.
110. Wesson, D.W., Donahou, T.N., Johnson, M.O., and Wachowiak, M. (2008). Sniffing Behavior of Mice during Performance in Odor-Guided Tasks. *Chem. Senses* 33, 581–596. <https://doi.org/10.1093/chemse/bjn029>.
111. Verhagen, J.V., Wesson, D.W., Netoff, T.I., White, J.A., and Wachowiak, M. (2007). Sniffing controls an adaptive filter of sensory input to the olfactory bulb. *Nat. Neurosci.* 10, 631–639. <https://doi.org/10.1038/nn1892>.
112. Wachowiak, M., and Shipley, M.T. (2006). Coding and synaptic processing of sensory information in the glomerular layer of the olfactory bulb. *Semin. Cell Dev. Biol.* 17, 411–423. <https://doi.org/10.1016/j.semcd.2006.04.007>.
113. Deschenes, M., Kurnikova, A., Elbaz, M., and Kleinfeld, D. (2016). Circuits in the Ventral Medulla That Phase-Lock Motoneurons for Coordinated Sniffing and Whisking. *Neural Plast.* 2016, 7493048. <https://doi.org/10.1155/2016/7493048>.
114. Findley, T.M., Wyrick, D.G., Cramer, J.L., Brown, M.A., Holcomb, B., Attaway, R., Yeh, D., Monasevitch, E., Nouboussi, N., Cullen, I., et al. (2021). Sniff-synchronized, gradient-guided olfactory search by freely moving mice. *Elife* 10, e58523. <https://doi.org/10.7554/eLife.58523>.
115. Baker, M. (2013). Neuroscience: Through the eyes of a mouse. *Nature* 502, 156–158. <https://doi.org/10.1038/502156a>.
116. Halliday, M.S. (2013). The influence of olfactory cues on exploratory behavior. *Psychon. Sci.* 9, 595–596. <https://doi.org/10.3758/bf03327906>.
117. Radvansky, B.A., and Dombeck, D.A. (2018). An olfactory virtual reality system for mice. *Nat. Commun.* 9, 839. <https://doi.org/10.1038/s41467-018-03262-4>.
118. Chen, W., Wang, Z., Ma, C., Ma, X., Meng, W., Yin, F., and Yang, Y. (2023). Tactile cues are important to environmental novelty during repeated open field tests. *Behav. Processes* 204, 104796. <https://doi.org/10.1016/j.beproc.2022.104796>.
119. Maaswinkel, H., and Whishaw, I.Q. (1999). Horning with locale, taxon, and dead reckoning strategies by foraging rats: sensory hierarchy in spatial navigation. *Behav. Brain Res.* 99, 143–152. [https://doi.org/10.1016/s0166-4328\(98\)00100-4](https://doi.org/10.1016/s0166-4328(98)00100-4).
120. Jiang, P.E., Lang, Q.H., Yu, Q.Y., Tang, X.-Y., Liu, Q.Q., Li, X.Y., and Feng, X.Z. (2019). Behavioral Assessments of Spontaneous Locomotion in a Murine MPTP-induced Parkinson's Disease Model. *J. Vis. Exp.* 7, 143. <https://doi.org/10.3791/58653-v>.
121. Zhou, Y., Ji, G., Yang, X., Chen, Z., and Zhou, L. (2023). Behavioral abnormalities in C57BL/6 mice with chronic ulcerative colitis induced by DSS. *BMC Gastroenterol.* 23, 84. <https://doi.org/10.1186/s12876-023-02718-2>.
122. Rosen, D.R., Siddique, T., Patterson, D., Figlewicz, D.A., Sapp, P., Hen-tati, A., Donaldson, D., Goto, J., O'Regan, J.P., Deng, H.X., et al. (1993). Mutations in Cu/Zn superoxide dismutase gene are associated with fa-miliar amyotrophic lateral sclerosis. *Nature* 362, 59–62. <https://doi.org/10.1038/362059a0>.
123. Prut, L., and Belzung, C. (2003). The open field as a paradigm to measure the effects of drugs on anxiety-like behaviors: a review. *Eur. J. Pharma-co.* 463, 3–33. [https://doi.org/10.1016/s0014-2999\(03\)01272-x](https://doi.org/10.1016/s0014-2999(03)01272-x).
124. Archer, J. (1973). Tests for emotionality in rats and mice: a review. *Anim. Behav.* 21, 205–235. [https://doi.org/10.1016/s0003-3472\(73\)80065-x](https://doi.org/10.1016/s0003-3472(73)80065-x).
125. Gould, T.D., Dao, D.T., and Kovacsics, C.E. (2009). The Open Field Test. In *Mood and Anxiety Related Phenotypes in Mice: Characterization Us-ing Behavioral Tests*, T.D. Gould, ed. (Humana Press), pp. 1–20. https://doi.org/10.1007/978-1-60761-303-9_1.
126. Li, H.Y., Zhu, M.Z., Yuan, X.R., Guo, Z.X., Pan, Y.D., Li, Y.Q., and Zhu, X.H. (2023). A thalamic-primary auditory cortex circuit mediates resil-i-ence to stress. *Cell* 186, 1352–1368.e18. <https://doi.org/10.1016/j.cell.2023.02.036>.
127. Lal, N.K., Le, P., Aggarwal, S., Zhang, A., Wang, K., Qi, T., Pang, Z., Yang, D., Nudell, V., Yeo, G.W., et al. (2023). Xiphoid nucleus of the midline thalamus controls cold-induced food seeking. *Nature* 627, 138–145. <https://doi.org/10.1038/s41586-023-06430-9>.
128. Sun, J., Yuan, Y., Wu, X., Liu, A., Wang, J., Yang, S., Liu, B., Kong, Y., Wang, L., Zhang, K., et al. (2022). Excitatory SST neurons in the medial paralemnisical nucleus control repetitive self-grooming and encode reward. *Neuron* 110, 3356–3373.e8. <https://doi.org/10.1016/j.neuron.2022.08.010>.
129. Elam, D., Zor, R., Szechtman, H., and Hermesh, H. (2006). Rituals, ste-reotypy and compulsive behavior in animals and humans. *Neurosci. Bio-behav. Rev.* 30, 456–471. <https://doi.org/10.1016/j.neubiorev.2005.08.003>.
130. Butler-Struben, H.M., Kentner, A.C., and Trainor, B.C. (2022). What's wrong with my experiment?: The impact of hidden variables on neuro-psychopharmacology research. *Neuropsychopharmacology* 47, 1285–1291. <https://doi.org/10.1038/s41386-022-01309-1>.
131. Nelson, R.J., Bumgarner, J.R., Walker, W.H., 2nd, and DeVries, A.C. (2021). Time-of-day as a critical biological variable. *Neurosci. Biobehav. Rev.* 127, 740–746. <https://doi.org/10.1016/j.neubiorev.2021.05.017>.
132. Pernold, K., Rullman, E., and Ulfhake, B. (2021). Major oscillations in spontaneous home-cage activity in C57BL/6 mice housed under

- constant conditions. *Sci. Rep.* 11, 4961. <https://doi.org/10.1038/s41598-021-84141-9>.
133. Valentinuzzi, V.S., Buxton, O.M., Chang, A.M., Scarbrough, K., Ferrari, E.A., Takahashi, J.S., and Turek, F.W. (2000). Locomotor response to an open field during C57BL/6J active and inactive phases: differences dependent on conditions of illumination. *Physiol. Behav.* 69, 269–275. [https://doi.org/10.1016/s0031-9384\(00\)00219-5](https://doi.org/10.1016/s0031-9384(00)00219-5).
134. Kalueff, A.V., Keisala, T., Minasyan, A., Kuuslahti, M., and Tuohimaa, P. (2006). Temporal stability of novelty exploration in mice exposed to different open field tests. *Behav. Processes* 72, 104–112. <https://doi.org/10.1016/j.beproc.2005.12.011>.
135. Tsao, C.H., Flint, J., and Huang, G.J. (2022). Influence of diurnal phase on behavioral tests of sensorimotor performance, anxiety, learning and memory in mice. *Sci. Rep.* 12, 432. <https://doi.org/10.1038/s41598-021-03155-5>.
136. Avni, R., Zadicario, P., and Eilam, D. (2006). Exploration in a dark open field: a shift from directional to positional progression and a proposed model of acquiring spatial information. *Behav. Brain Res.* 171, 313–323. <https://doi.org/10.1016/j.bbr.2006.04.006>.
137. Redlin, U. (2001). Neural basis and biological function of masking by light in mammals: suppression of melatonin and locomotor activity. *Chronobiol. Int.* 18, 737–758. <https://doi.org/10.1081/cbi-100107511>.
138. Aldarondo, D., Merel, J., Marshall, J.D., Hasenclever, L., Klibaite, U., Gelalis, A., Tassa, Y., Wayne, G., Botvinick, M., and Ölveczky, B.P. (2024). A virtual rodent predicts the structure of neural activity across behaviors. *Nature* 632, 594–602. <https://doi.org/10.1038/s41586-024-07633-4>.
139. Ding, J.X., Rudak, P.T., Inoue, W., and Haeryfar, S.M.M. (2021). Physical restraint mouse models to assess immune responses under stress with or without habituation. *STAR Protoc.* 2, 100838. <https://doi.org/10.1016/j.xpro.2021.100838>.
140. McLean, A.C., Valenzuela, N., Fai, S., and Bennett, S.A.L. (2012). Performing vaginal lavage, crystal violet staining, and vaginal cytological evaluation for mouse estrous cycle staging identification. *J. Vis. Exp.* e4389, e4389. <https://doi.org/10.3791/4389>.
141. Tseng, Y.T., Zhao, B., Ding, H., Liang, L., Schaeck, B., and Wang, L. (2023). Systematic evaluation of a predator stress model of depression in mice using a hierarchical 3D-motion learning framework. *Transl. Psychiatry* 13, 178. <https://doi.org/10.1038/s41398-023-02481-8>.
142. Han, Y., Huang, K., Chen, K., Pan, H., Ju, F., Long, Y., Gao, G., Wu, R., Wang, A., Wang, L., and Wei, P. (2022). MouseVenue3D: A Markerless Three-Dimension Behavioral Tracking System for Matching Two-Photon Brain Imaging in Free-Moving Mice. *Neurosci. Bull.* 38, 303–317. <https://doi.org/10.1007/s12264-021-00778-6>.
143. Endres, D.M., and Schindelin, J.E. (2003). A new metric for probability distributions. *IEEE Trans. Inf. Theory* 49, 1858–1860. <https://doi.org/10.1109/tit.2003.813506>.
144. Chang, C.-C., and Lin, C.-J. (2011). Libsvm. *ACM Trans. Intell. Syst. Technol.* 2, 1–27. <https://doi.org/10.1145/1961189.1961199>.
145. Breiman, L. (2001). Random forests. *Mach. Learn.* 45, 5–32. <https://doi.org/10.1023/a:1010933404324>.

STAR★METHODS

KEY RESOURCES TABLE

REAGENT or RESOURCE	SOURCE	IDENTIFIER
Chemicals, peptides, and recombinant proteins		
Giemsa stain solution	Solarbio Life Science	Cat# G1020; RRID:N/A
Deposited data		
Behavioral data	This paper	Zenodo Data: https://zenodo.org/records/10037411
Original code	This paper	https://github.com/Feng-Wang-Research-Group/The-hierarchical-behavioral-analysis-framework
Experimental models: Organisms/strains		
C57BL/6J	Zhejiang, Vital River Laboratory Animal Technology Co., Ltd. Zhejiang, China	RRID:IMSR_JAX:000664
Software and algorithms		
BehaviorAtlas Analyzer 1.0 ³¹	Shenzhen Bayone BioTech Co., Ltd. Shenzhen, China	https://behavioratlas.tech/
BehaviorAtlas Capture 1.0 ³¹	Shenzhen Bayone BioTech Co., Ltd. Shenzhen, China	https://behavioratlas.tech/
OLYMPUS OlyVIA 2.9	Olympus Software Imaging Solutions	https://www.olympus-sis.com/
GraphPad Prism 9.5	GraphPad Software Inc	https://www.graphpad.com/scientific-software/prism/ ; RRID: SCR_002798
Python 3.9	Python Software Company	https://www.python.org ; RRID: SCR_008394
Motionmapperpy ³⁰	Gordon Berman's lab	https://github.com/bermanlabemory/motionmapperpy
Statsmodels 0.13.5	Python module	https://www.statsmodels.org/stable/index.html
NetworkX 2.8.4	Python module	https://networkx.org
scikit-learn 1.2.1	Python module	https://scikit-learn.org/1.5/index.html
scipy 1.10.0	Python module	https://scipy.org/
Other		
BehaviorAtlas Capture Equipment	Shenzhen Bayone BioTech Co., Ltd. Shenzhen, China	https://behavioratlas.tech/
Infrared light	Thinker tech nanjing bioscience Inc.	Cat# QAXK-660730nmX; RRID: N/A
RealSense D435	Intel	https://www.intelrealsense.com/depth-camera-d435/

EXPERIMENTAL MODEL AND STUDY PARTICIPANT DETAILS

Mice

All procedures were performed according to guidelines established by the Chinese Council on Animal Care, approved by the Animal Care Committee of the Shenzhen Institutes of Advanced Technology, Chinese Academy of Sciences (IACUC No. SIAT-IACUC-20221209-ZKYSZXJJSYJY-RZC-WF-A2072-02). The animals used in this study were adult C57BL/6J mice (male: $n = 46$, female: $n = 46$) aged 9–12 weeks. Mice were grouped-housed (4–5 mice per cage, randomly assigned) on a standard 12-h light cycle (starting at 8:00, zeitgeber time, ZT0 = 8:00, ZT12 = 20:00) at 22–25°C with *ad libitum* access to food and water. Mice were habituated to the animal facility for at least one week and gently handled for 5 min/day for 7 consecutive days before the behavioral test.

METHOD DETAILS

Apparatus

To collect unobstructed behavioral data for elaborate analysis, we used a multi-view video capture device to record animal behaviors³¹ (Figures 1A and S1). Briefly, a 50 × 50 × 50 cm transparent acrylic square enclosure with white ground was placed at the center

of a $90 \times 90 \times 75$ cm support framework. A 56-inch screen was fixed on the top of the shelf, facing downwards, to provide stable 85 lux white light in the light-on recording. For the light-off recording, the screen was turned off and infrared light (Thinkerbiotech, Nanjing, China) was used. Four cameras (Inter, RealSense D435) were mounted on the supporting pillars, finely tuning the angle to capture a clear and complete view of the arena for each camera. Mouse behavior images were simultaneously acquired by four cameras at 30 Hz, 640×480 px, controlled by BehaviorAtlas Capture (version 1.01, Shenzhen Bayone BioTech Co.).

Experimental design and randomization

The experiments were conducted in two conditions: Naive (freely moving in a home cage with *ad libitum* access to food and water.) and acute stress (AS, 12-h overnight restraint before behavioral testing). The AS group mice underwent the experiment at 8:30-9:30, while the untreated mice were tested in three different periods: 8:00-12:00, 14:00-18:00 and 20:00-24:00. During the morning and afternoon experiments, the light was kept on. During nighttime, tests were conducted under both the light-on and light-off conditions. For the untreated group, three mice were randomly assigned in each experiment session (e.g., 14:00-18:00) and maintained a sex balance as possible. Mice with inaccurate recordings or those that fell outside the predetermined experimental time frame were excluded from the analysis.

Acute restraint stress model¹³⁹

The polycarbonate restrainer was composed of a small tube (93 mm length with a diameter of 30mm and a slit in the closed side panel) and an adjustable funnel head retainer. The mouse was placed into the tube through the open side and its tail was pulled out from the slit to reduce the excrement on its body. Subsequently, the head retainer was inserted into the tube and fastened after carefully adjusting the space to restrict mouse movement without causing pain, constriction, or suffocation.¹³⁹ Before the lights went off at 20:00, mice were transferred to the behavioral testing room and individually confined in a restrainer overnight during the nocturnal phase (from 20:00 until 8:00 on the following day). Before the behavioral testing, mice were allowed to habituate to light in a restraint state for an external 30 min. Spontaneous behavior was immediately recorded upon the mouse being released in the open-field arena.

Spontaneous behavioral procedure

Before the behavioral test, each animal was acclimated to the testing room for 30 min. To ensure equal habituation time, only the mouse awaiting testing would be individually isolated and brought to the testing room 30 min ahead of time. The mouse was then placed into the arena, and their spontaneous behavior was recorded for 60 min. After the behavioral test, vaginal smears were performed within 10 min to determine the female estrous cycle.¹⁴⁰ The arena was thoroughly cleaned with a 75% ethanol solution and allowed air dry before introducing the next mouse.

Behavioral data processing

Unsupervised clustering

BehaviorAtlas Analyzer (Version 1.01, Shenzhen Bayone BioTech Co.) was used to quantify spontaneous behavioral phenotypes³¹ (Figure S1). First, pose estimation, tracking 16 key body points of the mouse from four-view synchronized videos separately. To improve the performance of pose estimation, we manually labeled 2500 images for each training model (RGB and Infrared model). Second, the mouse's 3D skeleton is reconstructed, generating 3D body coordinates through 2D pose estimation combined with camera calibration information. Third, behavior segmentation, consecutive behavior was dynamically split into numerous movement fragments based on their skeleton kinematics features. Fourth, low-dimensional embedding and clustering, similar movement fragments grouped by hierarchical clustering and then randomly assigned a digital label (unsupervised movement modules).

Supervised movement annotation

To identify the movement phenotypes, we randomly selected and visually inspected 100 video clips of each movement and then combined movement modules with similar behavioral significance. (e.g., left-side grooming, right-side grooming, and face grooming were combined as "grooming"). Finally, we identified 15 basic movements of spontaneous behavior in the open field, referencing the previous studies^{31,141,142} and the Mouse Ethogram database (www.mousebehavior.org). Further, these 14 movements were categorized as 4 clusters (Table S1; Figure S2).

Movement label correction

Due to obstacles and insufficient frame rates, the spatial positioning of body key points in pose estimation may fluctuate, leading to reduced accuracy in recognizing low-speed movements like pausing and grooming. Furthermore, the BehaviorAtlas analysis framework did not incorporate spatial position information, making it challenging to distinguish movements with similar postures but occur in distinct positions, such as rearing and climbing. To enhance the accuracy of movement recognition, we extract the core movement features, including horizontal and vertical velocity, body length (distance from nose to root-tail), spine curvature, the positions of the front claws, duration, etc. (Table S2), to finely amend the movement label. The adjustment criteria are as follows: 'sniffing' would be reclassified as 'pausing' if the average horizontal velocity is below 15 mm/s and the duration of this movement exceeds 5 s; 'grooming' would be relabeled as 'scratching' if the average height of either hind claw exceeds that of the nose; 'climbing' would be redefined as 'rearing' if the average position of the front claws is more than 3 cm away from the wall; movement with an average height of

dorsal region over 80 mm was categorized as jumping. These adjustments were based on the movement labels assigned by BehaviorAtlas through manual annotation.

Posture spectrum mapping

To standardize the representation of posture diversity, we use MotionMapper³⁰ (<https://github.com/bermanlabemory/motionmapperpy>) to embed the posture feature into a Uniform Manifold Approximation and Projection (UMAP) space. Initially, the 3D skeleton, consisting of the 3D coordinates of 16 key points, was aligned based on the dorsal point and rotation to ensure consistent body orientation at each time frame. This process resulted in a 48-dimensional time-series array that enriched the instantaneous pose representation of each frame. These time series were then transformed into spectrograms using Continuous Wavelet Transform (CWT) with the Morlet wavelet as the mother wavelet. A total of 30 scales were selected to cover dyadically spaced center frequencies ranging from 1 to 15 Hz. The generated spectrograms were utilized to construct spectral feature vectors, which were subsequently embedded into two dimensions using UMAP embedding. Finally, we estimated the frequency of specific poses by calculating the probability distribution across this two-dimensional space (Figure 1C) and proceeded to map the movement labels obtained from BehaviorAtlas onto the posture spectrum map (Figure 1D).

Jensen-Shannon divergence (JSD) analysis

Jensen-Shannon divergence (JSD) is a way to measure the similarity between two probability distributions.¹⁴³ It is a symmetric and smoothed version of Kullback-Leibler divergence (KLD), ranging from 0–1, with 0 indicating that the two distributions are identical, and 1 indicating that they have no overlap. The JSD is defined as:

$$JSD(P\|Q) = \frac{KL\left(P\|\frac{(P+Q)}{2}\right)}{2} + \frac{KL\left(Q\|\frac{(P+Q)}{2}\right)}{2}$$

Here, P and Q are two probability distributions, and $KL(P\|Q)$ is calculating the KLD between P and Q, defined as $KLD(P\|Q) = \sum_{x \in X} P(x)\log\left(\frac{P(x)}{Q(x)}\right)$.

The dissimilarity of each mouse was calculated as JSD for all possible pairwise combinations of the candidate dataset. The figures and legends indicate comparisons between specific experiment groups (Figure 1E).

Principal component analysis (PCA)

To represent the behavioral features of mice in a lower-dimensional space, we utilized the principal component analysis (PCA) to reduce 14-dimensional movement fractions into 2-dimensional space (Figure 1F). Subsequently, we used the support vector machine (SVM) to generate the decision boundary,¹⁴⁴ facilitating the segregation of data points belonging to different groups.

Supervised learning classifier

In this study, we used Random Forest algorithms¹⁴⁵ to validate the sufficient of selected features in classifying or predicting samples. Random forest classifiers were trained on group-based movement fractions or one specific behavioral metric to determine whether the behavioral repertoires were distinct for each group (Figures 1G and S3B). Other random forest classifiers were trained on the ratio of sniffing to grooming, using both movement fraction and movement frequency, to evaluate this relationship's effectiveness in distinguishing each group's behavioral state (Figure 2E). To examine the uniqueness of each movement, another classifier was trained on core postural and kinematic features (Figure S2D). The performance of the classifier models was evaluated via stratified K-Fold cross-validation ($k = 10$), and the final confusion matrix was generated from the cumulative data across all folds.

Posture and kinematics analysis

The skeleton diagrams representing each movement were generated by averaging the position of the aligned skeleton of that movement, while the heatmap indicating activity in specific body parts was visualized using the 'mpl_scatter_density' Python package. Gaussian kernel density estimation was used to calculate the probabilistic density of each movement parameter, and the resulting stacked density plot was created using the 'joyplots' Python package (Figures 2A, 2D, and 2F). The stride cycle was determined by analyzing periodic variations (stride frequency) in the distance (stride size) between the front claws and hind claws (Figure 2B). Spine curvature in the top view or in 3D space was calculated by measuring the angle formed by the nose, neck, dorsal, and root tail (Figures 2C and 2E). Head direction is defined as the vector's orientation formed by the head and dorsal points to the angle between the dorsal and tail base points (Figure 2F). The body stretching value for a specific movement represents the average total distances between each pair of the 16 skeletal points, while the body stretching index is the ratio of the average body stretching value for each movement to the average body stretching value during sniffing in naive mice (Figure 2G).

The sniffing-to-grooming ratio

The sniffing-to-grooming ratio was determined by dividing the sniffing movement fraction by the grooming movement fraction or by dividing the sniffing movement frequency by the grooming frequency (Figure 3D). The specific calculation method, which includes data from various periods and regions, was outlined in the figure legend. If either sniffing or grooming were not observed in a particular time and region for a mouse, one-tenth of the minimum value would be assigned to that mouse (Figures 3D and 5G).

Occurrence time distribution of movements

To represent the movement occurrence pattern across 60 min, we calculate each movement's fraction in every minute (Figure 4A). To investigate the temporal variation within each movement, we extracted each movement independently and analyzed their occurrence time distribution in 60 min. We calculated $T_i = \frac{M_i}{M_{Total}}$, $i \in [1, 60]$ for a specific movement fraction in every minute, and then averaged each mouse in the same group to give a single value indicating the overall occurrence time percentage in that minute. We also

evaluated the linear relationship between movement occurrence probability and the experiment running time by calculating the Pearson correlation coefficient (Figure 4A).

The similarity of behaviors in the time course

To estimate the similarity of behavioral repertoire across different time intervals of the experiment, we segmented the 60-min behavior data into every 5-min block. Then we calculated the pairwise correlation distance of behavior blocks using a 15-dimensional movement vector for each mouse. The population behavior similarity of a group was determined by averaging the distance matrix generated by each mouse (Figure 4C). To further investigate the contributions of movements in diversifying behaviors, we compared the changing rate in movement clusters according to the bifurcation point identified in the distance matrix (Figure 4D).

Normalized dorsal coordinates and estimated mice's spatial preference

To obtain the accurate location of the mice, we used a custom Python script to amend and normalize the dorsal coordinates of each mouse. After rotation, alignment, and scaling, the origin was set as (0,0). Four corner points of the enclosure were calibrated as (-250, 250), (-250,250), (250, 250), and (-250, -250), resulting in a consistent coordinate system for all data points (Figure S8A). For each moment, the distance of a mouse to the center was calculated as:

$$d_t = \sqrt{(x_t - x_{\text{origin}})^2 + (y_t - y_{\text{origin}})^2}$$

and the normalized distance from the center was defined as $d_N = \frac{d_t}{d_{\max}}$, where $d_{\max} = 250 \times \sqrt{2}$, which is the distance from the corner to the center (Figure 5B).

Next, we estimated the preference regions of mice by analyzing their location distribution (Figures 5C and S8B). We partitioned the arena into a grid of 100×100 cells (5 mm^2 each) and transformed the data into a density heatmap by counting the number of points (dorsal coordinates) landing within these cells. To mitigate the influence of initial placement on spatial preference, we performed 1000 random rotations (n) of the density heatmap by $n \times 90$ degrees to mimic the activity data from various initial positions. The representative spatial distribution of a mouse was determined by averaging the values across the 1000 datasets. Then, we assigned a square frame with a side length of S that expanded from the center and calculated the standard variance (std) of the occupancy density of cells within the frame. To pinpoint where the square frame (S) began to exhibit acceleration in density differentiation, we further calculated the change rate of density variance and identified the 10% peak prominent was the growth acceleration point. Extension lines from the square frame at this point can divide the arena into three zones: corner, periphery, and center (Figure 5D). Above, we proposed a data-driven region-dividing method for a $50 \text{ cm} \times 50 \text{ cm}$ square open-field arena, which was found to be more precise in indicating the preference regions of mice.

Movement transition probability

To analyze movement transition probability, each movement was considered a state in the probabilistic graphical model, and each movement fragment was treated as an event, regardless of its duration (Figure 6A). Probabilities of states were approximately calculated based on the number of movement events, while state transition probabilities were estimated based on the frequency of the previous movement event to the next one. Only transition probabilities larger than 0.05 would be plotted in the state transition map and the difference matrix (Figure 6B). The differences in transition probabilities between the two groups were represented by the difference between the average transition probabilities (Figure 6D). The same approach was used to analyze transition probability among clusters and the difference in transition probability between compare groups. The entropy rate of transition probability was calculated as: $H = - \sum A_{ij} \log A_{ij}$, using the `scipy.stats.entropy` module in Python (Figure 6E).

Identify the nodes in the movement transition network

Centralities of movements in the transition network were used to estimate their importance in action switching. Here, we calculated degree centrality (the number of connections), closeness centrality (the inverse of the sum of shortest path distances from the node to all other nodes), and betweenness centrality (the number of shortest paths between pairs of nodes that pass through a particular node) of each movement using the 'NetworkX' packages in Python (Figure 6F). We normalized and summed up the centralities, then picked up the top 4 nodes and analyzed their connection properties (Figure 6G).

Movement duration probability

We estimated the probability of movement duration within the specific observed time window by using an adaptive kernel density estimator (KDE) to analyze the density distribution of movement durations. Given a set of finite date samples, $\{x_1, x_2, \dots, x_n\}$ are independent movement durations. At any given point \bar{x} , the density probability could be estimated as:

$$P(\bar{x}) = \frac{1}{nh} \sum_{i=1}^n K\left(\frac{\bar{x} - x_i}{h}\right)$$

where K is the kernel and h is the bandwidth. Here the bandwidth for each input dataset was calculated by 'sklearn.cluster.estimate_bandwidth' module.

Predicted movement sequences

To characterize the dynamic behavior patterns of mice, we estimated the transition and duration probabilities of each movement for every 5-min time window. According to these probabilities, we generated movement sequences by a simple formula: the next

movement was predicted based on the current movement transition probability. Then the next movement became the current movement, and its duration was estimated from the current movement duration probability ([Figure 7A](#)).

Time series data analysis

The cluster fraction (%) was decomposed into trend, seasonal varying, and residuals by additive mode on ‘statsmodels.tsa.seasonal’ module in Python. The trend component represents the long-term progression of the data, the seasonal component captures repetitive fluctuations occurring at regular intervals due to seasonal effects, and the residuals account for random variations or anomalies. The trend could represent the dynamics of exploration and maintenance force ([Figure S10D](#)).

QUANTIFICATION AND STATISTICAL ANALYSIS

Statistical analysis

The number of biological replicates in each group varied depending on the experiment and was indicated in figure legends. Data from male and female mice were included in the main graphs and presented as mean \pm SEM, unless otherwise specified. Before statistical analysis, the Shapiro-Wilk test ($n \leq 50$) and Kolmogorov-Smirnov test ($n > 50$) were used to assess the normality of the data distribution. For normally distributed data, statistical analyses were conducted using unpaired two-tailed Student’s t-test with Welch’s correction when comparing two populations, and one-way or two-way ANOVA tests with Bonferroni’s multiple comparisons when comparing multiple groups. For non-normally distributed data, statistical analyses were performed using the non-parametric Mann-Whitney test with Bonferroni-Dunn multiple comparisons. All statistical analyses were performed using GraphPad Prism 9.5 (GraphPad Software Inc.). The statistical significance threshold was set at $\alpha = 0.05$ (* $p < 0.05$; ** $p < 0.01$; *** $p < 0.001$), and p values are provided in figure legends. A custom Python script was utilized to analyze the differences in movement transition and postures through a permutation test (10,000 iterations), comparing mean value disparities between the two groups. Source data and detailed statistical analyses can be found in [Table S3](#).